2016291 GSA Data Repository

The Neogene de-greening of Central Asia

Jeremy K. Caves, Danielle Y. Moragne, Daniel E. Ibarra, Bolat U. Bayshashov, Yuan Gao, Matthew M. Jones, Aizhan Zhamangara, Anastasia V. Arzhannikova, Sergey G. Arzhannikov, and C. Page Chamberlain

Contents:

1) Section Details

1.1 Zaysan Basin, Kazakhstan

We collected 77 samples from the Neogene type-section in the Zaysan Basin, which lies along the Kalmakpay River in the southeast of the basin (47.4°N; 84.4°E). The sediments in this basin were classified into svitas (Sv.; similar to, but not strictly identical to formation) by Borisov (1963), and these divisions were maintained most recently by Lucas et al. (2000). The upper Neogene comprises ~200 m of pedogenically-altered, carbonate-rich redbeds, including the lower Kalmakpay Sv. and the upper Karabulak Sv. Kalmakpay Sv. sediments are primarily mudstones that dip ~20° NE and are separated from the yellowish sands of the underlying, lacustrine Sarybulak Sv. by an unconformity. The overlying Karabulak Sv. is coarser, with multiple pebble conglomerates and cross-bedded sandstones that cut into pedogenic facies, and dips ~10° NE. Throughout the basin, this sequence is capped by the "Gobi Conglomerate" (Berkey and Morris, 1923), which is regarded as a Quaternary deposit (Lucas et al., 2009) and from which we collected five samples of carbonate-rich cement.

The ages of these sediments are constrained by biostratigraphy and magnetostratigraphy, which was reviewed most recently by Lucas et al. (2009). The Sarybulak Sv. (from which we recovered no carbonate-rich samples) is assigned to the Tunggurian Asian Land Mammal Age (ALMA) (13.7-11.1 Ma) (Kowalski and Shevyreva, 1997). The Karabulak Sv. contains an abundant collection of "Hipparion" fauna, which is correlated with the latest Turolian (8.7-5.3 Ma; latest Baodean ALMA) (Sotnikova et al., 1997; Vangengeim et al., 1993; Lucas et al., 2009), though the very upper portion of the Karabulak Sv. may be early Pliocene. The intervening Kalmakpay Sv. is not as clearly constrained by mammal fossils, yet is a separate unit from the overlying Karabulak Sv. Following Vangengeim et al. (1993) and Lucas et al. (2009), we therefore place the lower boundary in the late Sarmatian (12.7-11.6 Ma) and the upper boundary in the lower Baodean ALMA. Regardless of the precise timing of these svitas, the entire upper Neogene sequence occurs within the upper Miocene and lowest Pliocene, excepting the five samples from the Gobi Conglomerate, which are placed within the Quaternary bin.

1.2 Erlian Basin, Inner Mongolia, China

We collected 89 carbonate-rich samples from four well-studied localities in the Erlian Basin that span the Miocene: Aoerban, Aletexire, Moergan, and Baogeda Ula. Here, we briefly review the sedimentology and age constraints for these sections, but refer the reader to more detailed sedimentological, paleontological and magnetostratigraphic studies in Wang et al. (2003; 2009) and Qiu et al. (2006; 2013). Though the following age constraints are uncertain, our analysis focuses on large time bins. The following sections all lie within either the lower or upper Miocene bins that we use in the main text. We only attempt to assign ages to these samples to calculate soil respiration (as detailed in DR Section 3).

The stratigraphically lowest locality is the Aoerban Formation (43.3°N; 113.9°E), which has been biostratigraphically constrained to the Early Miocene (Wang et al., 2009; Qiu et al., 2013) and from which we collected 29 samples. The entire formation is composed of fine-grained sediments that have been extensively pedogenically altered. Following the sedimentology of Wang et al. (2009), we collected 18 samples from the Lower Red Member, 3 samples from the Middle Green Member, and 7 samples from the Upper Red Member. Following Qiu et al. (2013), we place these samples stratigraphically in the Early Miocene, with the top of the Upper Red Member representing the boundary between the Early and Middle Miocene (16 Ma).

Both the Moergan (43.7°N; 112.9°E) and Aletexire (43.8°N; 113.1°E) sections are situated within the Tunggar Tableland and are estimated to lie within the Middle Miocene (Qiu et al., 2013). Both have been magnetostratigraphically constrained by Wang et al. (2003), which has been updated by Qiu et al. (2013). The Moergan locality, from which we collected 17 samples, consists primarily of channel sands at the base, which transition to pedogenically-altered mudstones in the upper part of the section. At the very base of the section, there is a laterally extensive freshwater bivalve bed, which we exclude from our compilation. The lower part of the Aletexire section consists of mature, thick paleosols with extensive caliche layers and root casts. The upper part of the section consists of pedogenically-altered mudstones that overlap stratigraphically with the Moergan locality (Wang et al., 2003). We collected 22 samples from the Aletexire section. Following Qiu et al. (2013), we treat the lower Aletexire as having been deposited between 15 and 14 Ma, while the upper Aletexire and Moergan sediments were deposited between 13 Ma and 11 Ma.

The highest locality stratigraphically that we sampled is Baogeda Ula (44.1°N; 114.60°E), from which we collected 21 samples. The section is capped by a basalt that Qiu et al. (2006) determined is 7.1 ± 0.5 Ma, based upon work by Luo and Chen (1990). The section consists primarily of channel sands, though the middle of the section comprises a thick, pedogenically-altered mudstone sequence. Following Qiu et al. (2013) and based upon biostratigraphic evidence, we place this section within the late Miocene and assume deposition between 8.5 and 7 Ma.

These sections are grouped and reported as "Erlian Basin" in the summary table (Table DR3).

1.3 Lake Baikal Sections

We collected 5 carbonate samples from two Neogene Formations on Olkhon Island in Lake Baikal. The Tagay Formation, the lowest of the formations, overlies the crystalline basement and Upper Cretaceous-Lower Oligocene weathering crust. It consists of continental and lacustrine deposits, including montmorillonite clays and paleosols, sands cemented by carbonates and gypsum, and thin layers of coal. The age of the Tagay Formation is constrained by biostratigraphy (Logachev, 1964), which was reviewed by Vislobokova (1990) and is assumed to be Lower to Middle Miocene (Mats et al., 2000; Mats et al., 2011). Given the large uncertainty in the age, we place these samples in our lower Miocene time bin (>14 Ma). The Tagay Sequence (53.15°N; 107.2°E), from which we collected 3 samples, represents a section of sub-parallel bedded continental deposits in the upper part of the Tagay Formation. At the very base of the section there is a layer of fine-grained carbonated sands. Upwards, there is an alteration of brown paleosols, fine-grained sands, and carbonate interlayers up to 0.3 m thick, which we interpret as thick caliche units. The paleosols include many lenses of carbonate. We collected two samples from the lowest and the uppermost carbonate interlayers of the section and one sample from a carbonate lens in the paleosol layer in the middle of the section. The samples show little variance in $\delta^{13}C$, though we note that we only have 3 samples from this locality.

The Sasa formation uncorformably overlies the Tagay Formation. It consists of lacustrine clays, silts, sands, gravels and a facies of sub-aerial clays and paleosols that represent the first horizon of the Neogene red strata (Vorob'eva et al., 1987). The age of the Sasa Formation is based on biostratigraphy and paleomagnetic data and determined as Late Miocene to Early Pliocene (Mats et al., 2000). We collected two samples from the uppermost sequence of the sub-aerial facies assigned to the Early Pliocene. The Kharaldai section (53.25°N; 107.4°E) comprises red-cinnamonic 8-meter thick paleosols that overlie sub-aerial green montmorillonite clay at the base of the section. The paleosols are clay-rich and contain carbonates that increase in amount upward in the section (Vorob'eva et al., 1987). We collected two samples in the thin lens of carbonates in the upper part of the section.

2) Laboratory Methods

Samples were powdered using either a mortar and pestle or a Dremel. Stable carbon and oxygen isotope values of carbonates were obtained at the Stable Isotope Biogeochemistry Laboratory, Stanford University, using a Thermo Finnigan Gasbench interfaced with a Thermo Finnigan Delta Plus XL mass spectrometer via a Thermo Finnigan ConFlo III unit. Depending on the samples' carbonate content, between 200 and 5000 µg of sample powder was weighed into sealed vials that were flushed with He gas and reacted with ca. 0.25 ml of phosphoric acid (H_3PO_4) for 1 hour at 72 °C. External precision (1σ) of oxygen and carbon isotope data is generally <0.1‰, based upon repeated measurements of two internal laboratory standards (calibrated against NBS 18, NBS 19, and LSVEC). The $\delta^{13}C$ values are reported relative to VPDB; $\delta^{18}O$ values are reported relative to VSMOW. Results are reported in Table DR2.

3) Calculation of Soil Respiration Fluxes

To calculate soil respiration fluxes (as presented in Figure 2E-H, main text), we use equations 1 and 2 from the main text. The values we use for the parameters in these equations are listed in DR Table 1 and are widely-accepted values used in previous applications of the CO_2 diffusion-production model of Cerling (1984) (Cerling and Quade, 1993; Ekart et al., 1999; Breecker et al., 2010). For δ_o, we assume -25‰, except for samples from the Siwalik Fm., where the expansion of C_4 grasses is well-documented (Quade et al., 1989; Quade and Cerling, 1995; Sanyal et al., 2004). For these samples, we use published δ_o values from the same publications from which we use the $\delta^{13}C_c$ data. However, there are more $\delta^{13}C_c$ measurements from the Siwalik Fm. than δ_o measurements; therefore, we interpolate the δ_o measurements where necessary. Though there is evidence that C_4 vegetation also spread to the Loess Plateau (Passey et al., 2009; An et al., 2005; Zhang et al., 2003), the $\delta^{13}C_c$ values on the Loess Plateau are relatively low for the entire Neogene, though perhaps this is due to clastic carbonate contamination. Thus, even if δ_o was higher on the Loess Plateau due to the presence of C_4 vegetation, estimated soil respiration would be even higher to produce such low $\delta^{13}C_c$ values.

For the remaining samples in our compilation, we use -25‰ based upon two lines of evidence suggesting that this is a reasonable estimate for δ_o. First, a global compilation of soil organic matter $\delta^{13}C$ which co-occurs with soil carbonate produces an average value of -25‰ (Montañez, 2013). Second, model estimates of leaf $\delta^{13}C$ across Asia range from -28‰ to -23.5‰ (Suits et al., 2005). We further explore how changes in δ_o affect our estimate of soil respiration in DR Section 4 and DR Figure 5.

To constrain C_a, we use a compilation of published estimates of past atmospheric pCO_2 (Badger et al., 2013a; Badger et al., 2013b; Beerling and Royer, 2011; Bijl et al., 2010; Doria et al., 2011; Franks et al., 2014; Maxbauer et al., 2014; Pagani et al., 2009; Pagani et al., 2011; Zhang et al., 2013; Foster et al., 2012; Tripati et al., 2009; Bartoli et al., 2011; Seki et al., 2010) (Fig. DR1); however, to avoid circular constructs, we exclude paleosol-based estimates of pCO_2. There is large variability in this dataset, which is likely due to uncertainties in the proxy methods themselves, rather than true, high-frequency variations in atmospheric pCO_2 (Beerling and Royer, 2011). Thus, to smooth this record, we use an Epanechnikov kernel with a 1 Ma bandwidth (Epanechnikov, 1969) and the *np* package in R (Hayfield and Racine, 2008). To constrain δ_a, we use the estimates of Tipple et al. (2010) (Fig. DR2). Finally, we interpolate the smoothed C_a record and δ_a to the estimated age of each $\delta^{13}C_c$ measurement to calculate the soil respiration flux.

In the main text, we assume a spatially-invariant carbonate formation temperature (T) of 25°C to calculate δ_s from $\delta^{13}C_c$. We use this temperature given increasing evidence that soil carbonate forms during some of the hottest months of the year (June, July, and August in Asia) (Hough et al., 2014; Quade et al., 2013; Breecker et al., 2009). However, in DR Section 4, we also present an analysis where we use a spatially-varying temperature field to calculate δ_s from $\delta^{13}C_c$ (see also DR Figure 9). For the remaining parameters, we assume that, in carbonate-bearing soils, there is not substantial variability in these parameters and therefore use spatially-invariant values to estimate soil respiration (see also sensitivity analyses in DR Section 4 and DR Figures 3-9).

To convert the calculated soil respiration flux (ϕ_s) [mols/cm^3/s] into the standard areal flux measurement (SR) [mols/cm^2/s] that is typically considered in soil respiration studies (Bond-Lamberty and Thomson, 2010; Raich and Schlesinger, 1992), we integrate equation 2 over the depth of the soil (L):

$$SR = \phi_s \dot{z} - \phi_s \dot{z} e^{\left(-\frac{L}{\dot{z}}\right)} \qquad \text{(Eq. DR1).}$$

We report this areal flux measurement in the main text, converted to g C/m^2/yr. The R code used to calculate the mean $\delta^{13}C_c$ and the soil respiration flux is available at the Stanford Digital Repository (http://purl.stanford.edu/kk523mb1898).

Finally, because it is difficult to present uncertainty in maps of mean data, in Table DR3, we report uncertainty estimates for both $\delta^{13}C_c$ and for ϕ_s. For $\delta^{13}C_c$, we report the mean (used in producing Fig. 2A-D, main text) and 1 standard deviation. For ϕ_s, we first eliminate any negative estimates of ϕ_s as these are physically impossible and likely represent non-equilibrium fractionation between soil CO_2 and carbonate (Montañez, 2013) or inaccuracies in one of the parameters (*i.e.*, δ_o, T, etc.). We then calculate the mean ϕ_s (used in producing Fig. 2E-H, main text) and the 90% confidence interval (*i.e.*, the range from the 5% to 95% quantile). We report the 90% confidence interval in Table DR3 because the equations used to calculate ϕ_s do not lead to normally-distributed estimates; consequently, the errors are large. For example, as $\delta^{13}C_c$ approaches the theoretical fractionation between soil CO_2 and carbonate, the estimated ϕ_s increases exponentially. Thus, low $\delta^{13}C_c$ results in large uncertainty in estimated ϕ_s as these values approach the theoretical equilibrium fractionation between soil CO_2 and carbonate.

4) Sensitivity Calculations and Analyses

The estimated soil respiration fluxes (*SR*) presented in the main text are subject to uncertainty regarding the numerous parameters in equations 1 and 2 (main text) and equation DR 1. Because we present data spatially, it is difficult to visualize these uncertainties. Therefore, in DR Figures 3-9, we present sensitivity maps, whereby we change the value of one of the parameters and recalculate *SR* for each locality for the same time bins (*i.e.*, lower Miocene, upper Miocene, Pliocene, and Quaternary) as presented in the main text. We include the R code for these sensitivity analyses in the Stanford Digital Repository (http://purl.stanford.edu/kk523mb1898). Below, we discuss the parameters evaluated and the sensitivity of *SR* to changes in these parameters.

For these sensitivity tests, we evaluate the effect of 7 parameters on estimated *SR*: C_a, δ_a, δ_o, z, $\dot{z}$, L, and T. For each of these parameters, we vary the chosen parameter, while keeping all other parameters constant, and calculate the resulting *SR*. C_a and δ_a are both time-varying parameters; therefore, for these sensitivity tests, we use the high and low estimates as shown in DR Figures 1 and 2. To calculate the sensitivity of *SR* to the assumed carbonate formation temperature (T), we compare the results from the main text—which assume a spatially-invariant T of 25°C—with a spatially-varying temperature field. We use NCEP/NCAR Reanalysis II data (Kanamitsu et al., 2002) and interpolate the 2 m surface air temperature field to the pedogenic carbonate locality. For the T sensitivity analysis, we calculate *SR* assuming that carbonate formation temperatures reflect either annually-averaged temperatures or JJA-averaged temperatures (average surface air temperature of the summer season—June, July, and August). In each of the sensitivity map figures, we present two sensitivity analyses as well as the results from the main text in the center column, which are included for comparison purposes. We do not test the interaction of any of these parameters; instead, the focus of our sensitivity analysis is to identify the importance of single parameters and demonstrate that are results are robust, even given uncertainty in these parameters.

Throughout the entire Neogene, the spatial pattern of *SR* is not sensitive to any of the tested parameters (DR Figures 3-9). Interior Asia—comprising the Tarim and Qaidam basins—has much lower *SR* than surrounding regions in all time bins. In contrast, the temporal trends are somewhat sensitive to the assumed parameter value. For example, when higher C_a is used, upper Miocene *SR* estimates are consequently higher. This result reflects the fact that—at higher pCO_2—we model a higher *SR* to match the observed $\delta^{13}C_c$. There is growing evidence that mid-Miocene pCO_2 was higher than previously estimated (Bolton and Stoll, 2013; Bolton et al., 2016; Breecker and Retallack, 2014; Foster et al., 2012). Thus, higher C_a in the mid-Miocene would produce an even larger decrease in *SR* than presented in the main text (see DR Figure 3I-L).

SR is fairly insensitive to the assumed evolution of δ_a over the Neogene (DR Figure 4). In contrast, *SR* is more sensitive to the assumed value of δ_o (DR Figure 5), which is poorly constrained, except in the Siwalik Fm. For instance, if δ_o is higher than assumed in the main text (-23‰), *SR* is consequently greater in all time-slices, though the effect is most pronounced in the Miocene. Indeed, the "de-greening" trend is most pronounced if δ_o is higher than presented in the main text.

The depth of carbonate formation (z) influences *SR*, with lower (*i.e.*, shallower) depths resulting in higher *SR* (DR Figure 6). At shallower depths in the soil, high $\delta^{13}C$ atmospheric CO_2 has a greater influence on $\delta^{13}C_c$. Therefore, we model a higher *SR* to match the observed $\delta^{13}C_c$. This effect is not linear (Cerling, 1984; Cerling and Quade, 1993); thus, the sensitivity to changes in z is greater for formation depths above 50 cm than for formation depths below 50 cm in the soil. *SR* is also sensitive to the exact value of $\dot{z}$ (DR Figure 7) with the "de-greening" trend most pronounced if $\dot{z}$ is lower (15 cm) than presented in the main text. Unfortunately, there are few constraints on the value of $\dot{z}$. In the main text, we follow Cerling and Quade (1993) and use 25 cm. *SR* is relatively insensitive to the depth of the soil column (L) (DR Figure 8).

Finally, *SR* is most sensitive to the assumed temperature of carbonate formation (T) (DR Figure 9). Both the JJA-average and annual-average temperatures are generally lower than our assumed formation temperature of 25°C. A lower T produces a higher *SR* because a lower T has a greater ^{13}C fractionation during carbonate formation and, thus, a lower δ_s. However, despite this sensitivity, the same spatial and temporal trends are evident: interior Asia is surrounded by areas with higher *SR* and *SR* decreases into the Quaternary, particularly across Central Asia.

5) References

An, Z., Huang, Y., Liu, W., Guo, Z., Clemens, S., Li, L., Prell, W., Ning, Y., Cai, Y., Zhou, W., Lin, B., Zhang, Q., Cao, Y., Qiang, X., et al., 2005, Multiple expansions of C4 plant biomass in East Asia since 7 Ma coupled with strengthened monsoon circulation: Geology, v. 33, no. 9, p. 705–708, doi: 10.1130/G21423.1.

Badger, M.P.S., Lear, C.H., Pancost, R.D., Foster, G.L., Bailey, T.R., Leng, M.J., and Abels, H.A., 2013a, CO2 drawdown following the middle Miocene expansion of the Antarctic Ice Sheet: Paleoceanography, v. 28, no. 1, p. 42–53, doi: 10.1002/palo.20015.

Badger, M.P.S., Schmidt, D.N., Mackensen, A., and Pancost, R.D., 2013b, High-resolution alkenone palaeobarometry indicates relatively stable pCO2 during the Pliocene (3.3-2.8 Ma): Philosophical Transactions of the Royal Society A, v. 371, no. 20130094, doi: 10.1098/rsta.2013.0094.

Bartoli, G., Hönisch, B., and Zeebe, R.E., 2011, Atmospheric CO2 decline during the Pliocene intensification of Northern Hemisphere glaciations: Paleoceanography, v. 26, no. 4, doi: 10.1029/2010PA002055.

Beerling, D.J., and Royer, D.L., 2011, Convergent Cenozoic CO2 history: Nature Geoscience, v. 4, no. 7, p. 418–420, doi: 10.1038/ngeo1186.

Berkey, C.P., and Morris, F.K., 1923, Geology of Mongolia—a reconnaissance report based on the investigations of the years 1922–1923: American Museum of Natural History, New York, NY, USA.

Bijl, P.K., Houben, A.J.P., Schouten, S., Bohaty, S.M., Sluijs, A., Reichart, G.-J., Sinninghe Damsté, J.S., and Brinkhuis, H., 2010, Transient Middle Eocene atmospheric CO_2 and temperature variations: Science, v. 330, no. 6005, p. 819–821, doi: 10.1126/science.1193654.

Bolton, C.T., Hernández-Sánchez, M.T., Fuertes, M.-Á., González-Lemos, S., Abrevaya, L., Mendez-Vicente, A., Flores, J.-A., Probert, I., Giosan, L., Johnson, J., and Stoll, H.M., 2016, Decrease in coccolithophore calcification and CO2 since the middle Miocene: Nature Communications, v. 7, p. 10284, doi: 10.1038/ncomms10284.

Bolton, C.T., and Stoll, H.M., 2013, Late Miocene threshold response of marine algae to carbon dioxide limitation: Nature, v. 500, no. 7464, p. 558–562, doi: 10.1038/nature12448.

Bond-Lamberty, B., and Thomson, A., 2010, A global database of soil respiration data: Biogeosciences, v. 7, no. 6, p. 1915–1926, doi: 10.5194/bg-7-1915-2010.

Borisov, B.A., 1963, [The stratigraphy of the Upper Cretaceous and of the Paleogene-Neogene of the Zaysan Depression]. Stratigrafiya verkhnego mela i paleogen-neogena Zaysanskoy vvpadiny. Materiali po geologii i poleznym iskopayemym Altaya i Kazakhstana: Trudy VSEGEI i Gos. Geol. Komenta, v. 94, p. 11–75.

Breecker, D.O., and Retallack, G.J., 2014, Refining the pedogenic carbonate atmospheric CO2 proxy and application to Miocene CO2: Palaeogeography, Palaeoclimatology, Palaeoecology, v. 406, p. 1–8, doi: 10.1016/j.palaeo.2014.04.012.

Breecker, D.O., Sharp, Z.D., and McFadden, L.D., 2010, Atmospheric CO2 concentrations during ancient greenhouse climates were similar to those predicted for A.D. 2100.: Proceedings of the National Academy of Sciences of the United States of America, v. 107, no. 2, p. 576–80, doi: 10.1073/pnas.0902323106.

Breecker, D.O., Sharp, Z.D., and McFadden, L.D., 2009, Seasonal bias in the formation and stable isotopic composition of pedogenic carbonate in modern soils from central New Mexico, USA: Geological Society of America Bulletin, v. 121, no. 3-4, p. 630–640, doi:

10.1130/B26413.1.
Caves, J.K., Bayshashov, B.U., Zhamangara, A., Ritch, A.J., Ibarra, D.E., Sjostrom, D.J., Mix, H.T., Winnick, M.J., and Chamberlain, C.P. Late Miocene uplift of the Tian Shan and Altai and reorganization of Central Asia climate: GSA Today, p. in review.
Caves, J.K., Sjostrom, D.J., Mix, H.T., Winnick, M.J., and Chamberlain, C.P., 2014, Aridification of Central Asia and Uplift of the Altai and Hangay Mountains, Mongolia: Stable Isotope Evidence: American Journal of Science, v. 314, no. 8, p. 1171–1201, doi: 10.2475/08.2014.01.
Cerling, T.E., 1984, The stable isotopic composition of modern soil carbonate and its relationship to climate: Earth and Planetary Science Letters, v. 71, no. 2, p. 229–240, doi: 10.1016/0012-821X(84)90089-X.
Cerling, T.E., and Quade, J., 1993, Stable Carbon and Oxygen Isotopes in Soil Carbonates, *in* Swart, P., Lohmann, K., McKenzie, J., and Savin, S. eds., Climate Change in Continental Isotopic Records, American Geophysical Union, Washington, DC, p. 217–231.
Charreau, J., Kent-Corson, M.L., Barrier, L., Augier, R., Ritts, B.D., Chen, Y., France-Lannord, C., and Guilmette, C., 2012, A high-resolution stable isotopic record from the Junggar Basin (NW China): Implications for the paleotopographic evolution of the Tianshan Mountains: Earth and Planetary Science Letters, v. 341-344, p. 158–169, doi: 10.1016/j.epsl.2012.05.033.
Currie, B.S., Rowley, D.B., and Tabor, N.J., 2005, Middle Miocene paleoaltimetry of southern Tibet: Implications for the role of mantle thickening and delamination in the Himalayan orogen: Geology, v. 33, no. 3, p. 181–184, doi: 10.1130/G21170.1.
Dettman, D.L., Fang, X., Garzione, C.N., and Li, J., 2003, Uplift-driven climate change at 12 Ma: a long δ18O record from the NE margin of the Tibetan plateau: Earth and Planetary Science Letters, v. 214, no. 1-2, p. 267–277, doi: 10.1016/S0012-821X(03)00383-2.
Ding, Z.L., and Yang, S.L., 2000, C3/C4 vegetation evolution over the last 7.0 Myr in the Chinese Loess Plateau: evidence from pedogenic carbonate d13C: Palaeogeography, Palaeoclimatology, Palaeoecology, v. 160, p. 291–299.
Doria, G., Royer, D.L., Wolfe, A.P., Fox, A., Westgate, J.A., and Beerling, D.J., 2011, Declining atmospheric CO2 during the late Middle Eocene climate transition: American Journal of Science, v. 311, no. 1, p. 63–75, doi: 10.2475/01.2011.03.
Ekart, D.D., Cerling, T.E., Montañez, I.P., and Tabor, N.J., 1999, A 400 Million Year Carbon Isotopte Record of Pedogenic Carbonate: Implications for Paleoatmospheric Carbon Dioxide: American Journal of Science, v. 299, p. 805–827.
Epanechnikov, V.A., 1969, Non-parametric estimation of a multivariate probability density: Theory of Probability & Its Applications, v. 14, no. 1, p. 153–158.
Foster, G.L., Lear, C.H., and Rae, J.W.B., 2012, The evolution of pCO2, ice volume and climate during the middle Miocene: Earth and Planetary Science Letters, v. 341-344, p. 243–254, doi: 10.1016/j.epsl.2012.06.007.
Franks, P.J., Royer, D.L., Beerling, D.J., Van de Water, P.K., Cantrill, D.J., Barbour, M.M., and Berry, J.A., 2014, New constraints on atmospheric CO2 concentration for the Phanerozoic: Geophysical Research Letters, v. 41, p. 4685–4694, doi: 10.1002/2014GL060457.
Gao, Y., Ibarra, D.E., Wang, C., Caves, J.K., Chamberlain, C.P., Graham, S.A., and Wu, H., 2015, Mid-latitude terrestrial climate of East Asia linked to global climate in the Late Cretaceous: Geology, v. 43, no. 4, p. 287–290, doi: 10.1130/G36427.1.
Garzione, C.N., Dettman, D.L., Quade, J., DeCelles, P.G., and Butler, R.F., 2000, High times on

the Tibetan Plateau: Paleoelevation of the Thakkhola graben, Nepal: Geology, v. 28, no. 4, p. 339–342, doi: 10.1130/0091-7613(2000)28<339:HTOTTP>2.0.CO;2.

Harrison, T.M., Copeland, P., Hall, S.A., Quade, J., Burner, S., Ojha, T.P., and Kidd, W.S.F., 1993, Isotopic Preservation of Himalya/Tibetan Uplift, Denudation and Climatic Histories of two Molasse Deposits: Journal of Geology, v. 101, no. 2, p. 157–175.

Hayfield, T., and Racine, J.S., 2008, Nonparametric econometrics: The np package: Journal of Statistical Software, v. 27, no. 5, doi: 10.1198/jasa.2001.s374.

He, T., Chen, Y., Balsam, W., Sheng, X., Liu, L., Chen, J., and Ji, J., 2012, Distribution and origin of protodolomite from the late Miocene-Pliocene Red Clay Formation, Chinese Loess Plateau: Geochemistry, Geophysics, Geosystems, v. 13, no. 6, p. Q06004, doi: 10.1029/2012GC004039.

Hoke, G.D., Liu-Zeng, J., Hren, M.T., Wissink, G.K., and Garzione, C.N., 2014, Stable isotopes reveal high southeast Tibetan Plateau margin since the Paleogene: Earth and Planetary Science Letters, v. 394, p. 270–278, doi: 10.1016/j.epsl.2014.03.007.

Hough, B.G., Fan, M., and Passey, B.H., 2014, Calibration of the clumped isotope geothermometer in soil carbonate in Wyoming and Nebraska, USA: Implications for paleoelevation and paleoclimate reconstruction: Earth and Planetary Science Letters, v. 391, p. 110–120, doi: 10.1016/j.epsl.2014.01.008.

Hough, B.G., Garzione, C.N., Wang, Z., Lease, R.O., Burbank, D.W., and Yuan, D., 2011, Stable isotope evidence for topographic growth and basin segmentation: Implications for the evolution of the NE Tibetan Plateau: Geological Society of America Bulletin, v. 123, no. 1-2, p. 168–185, doi: 10.1130/B30090.1.

Jiang, W., Peng, S., Hao, Q., and Liu, T., 2002, Carbon isotopic records in paleosols over the Pliocene in Northern China: Implication on vegetation development and Tibetan uplift: Chinese Science Bulletin, v. 47, no. 8, p. 687–690.

Kaakinen, A., Sonninen, E., and Lunkka, J.P., 2006, Stable isotope record in paleosol carbonates from the Chinese Loess Plateau: Implications for late Neogene paleoclimate and paleovegetation: Palaeogeography, Palaeoclimatology, Palaeoecology, v. 237, no. 2-4, p. 359–369, doi: 10.1016/j.palaeo.2005.12.011.

Kanamitsu, M., Ebisuzaki, W., Woollen, J., Yang, S.-K., Hnilo, J.J., Fiorino, M., and Potter, G.L., 2002, NCEP–DOE AMIP-II Reanalysis (R-2): Bulletin of the American Meteorological Society, v. 83, no. 11, p. 1631–1643, doi: 10.1175/BAMS-83-11-1631.

Kent-Corson, M.L., Ritts, B.D., Zhuang, G., Bovet, P.M., Graham, S.A., and Chamberlain, C.P., 2009, Stable isotopic constraints on the tectonic, topographic, and climatic evolution of the northern margin of the Tibetan Plateau: Earth and Planetary Science Letters, v. 282, no. 1-4, p. 158–166, doi: 10.1016/j.epsl.2009.03.011.

Kowalski, K., and Shevyreva, N.S., 1997, Gliridae (Mammalia: Rodentia) from the Miocne of the Zaisan Depression (Eastern Kazakhstan): Acta Zoologica Cracoviensia, v. 40, no. 2, p. 199–208.

Logachev, N.A., 1964, Stratigraphy. The Cenozoic (in Russian), *in* Florensov, N.A. ed., Geology of the USSR, Nedra, Moscow, p. 258–281.

Lucas, S.G., Aubekerov, B.Z., Dzhamangaraeva, A., Bayshashov, B.U., and Tyutkova, L.A., 2000, Cenozoic Lacustrine Deposits of the Ili Basin, Southeastern Kazakhstan, *in* Gierlowski-Kordesch, E. and Kelts, K. eds., Lake basins through space and time: AAPG Studies in Geology, p. 59–64.

Lucas, S.G., Emry, R.J., Bayshashov, B., and Tyutkova, L., 2009, Cenozoic Mammalian

Biostratigraphy and Biochronology in the Zaysan Basin, Kazakstan: Museum of Northern Arizona Bulletin, v. 65, p. 621–634.

Luo, X., and Chen, Q., 1990, Preliminary study on Geochronology for Cenozoic Basalts from Inner Mongolia: Acta Petrologica et Mineralogica, v. 9, no. 1, p. 34–46.

Macaulay, E.A., Sobel, E.R., Mikolaichuk, A., Wack, M., Gilder, S.A., Mulch, A., Fortuna, A.B., Hynek, S., and Apayarov, F., 2016, The sedimentary record of the Issyk Kul basin, Kyrgyzstan: climatic and tectonic inferences: Basin Research, v. 28, p. 57–80, doi: 10.1111/bre.12098.

Mats, V.D., Khlystov, O.M., De Batist, M., Ceramicola, S., Lomonosova, T.K., and Klimansky, a., 2000, Evolution of the Academician Ridge Accommodation Zone in the central part of the Baikal Rift, from high-resolution reflection seismic profiling and geological field investigations: International Journal of Earth Sciences, v. 89, no. 2, p. 229–250, doi: 10.1007/s005310000094.

Mats, V.D., Shcherbakov, D.Y., and Efimova, I.M., 2011, Late Cretaceous-Cenozoic history of the Lake Baikal depression and formation of its unique biodiversity: Stratigraphy and Geological Correlation, v. 19, no. 4, p. 404–423, doi: 10.1134/S0869593811040058.

Maxbauer, D.P., Royer, D.L., and LePage, B.A., 2014, High Arctic forests during the middle Eocene supported by moderate levels of atmospheric CO2: Geology, v. 42, p. 1027–1030, doi: 10.1130/G36014.1.

Montañez, I.P., 2013, Modern soil system constraints on reconstructing deep-time atmospheric CO2: Geochimica et Cosmochimica Acta, v. 101, p. 57–75, doi: 10.1016/j.gca.2012.10.012.

Pagani, M., Huber, M., Liu, Z., Bohaty, S.M., Henderiks, J., Sijp, W., Krishnan, S., and DeConto, R.M., 2011, The role of carbon dioxide during the onset of Antarctic glaciation: Science, v. 334, p. 1261–1264, doi: 10.1126/science.1203909.

Pagani, M., Liu, Z., LaRiviere, J., and Ravelo, A.C., 2009, High Earth-system climate sensitivity determined from Pliocene carbon dioxide concentrations: Nature Geoscience, v. 3, no. 1, p. 27–30, doi: 10.1038/ngeo724.

Passey, B.H., Ayliffe, L.K., Kaakinen, A., Zhang, Z., Eronen, J.T., Zhu, Y., Zhou, L., Cerling, T.E., and Fortelius, M., 2009, Strengthened East Asian summer monsoons during a period of high-latitude warmth? Isotopic evidence from Mio-Pliocene fossil mammals and soil carbonates from northern China: Earth and Planetary Science Letters, v. 277, no. 3-4, p. 443–452, doi: 10.1016/j.epsl.2008.11.008.

Qiu, Z.-D., Wang, X., and Li, Q., 2006, Faunal succession and biochronology of the Miocene through Pliocene in Nei Mongol (Inner Mongolia): Vertebrata PalAsiatica, v. 44, no. 2, p. 164–181.

Qiu, Z.-D., Wang, X., and Li, Q., 2013, Neogene Faunal Succession and Biochronology of Central Nei Mongol (Inner Mongolia), *in* Wang, X., Flynn, L.J., and Fortelius, M. eds., Fossil Mammals of Asia: Neogene Biostratigraphy and Chronology, Columbia University Press, New York, p. 155–186.

Quade, J., Cater, J.M.L., Ojha, T.P., Adam, J., and Harrison, T.M., 1995, Late Miocene environmental change in Nepal and the northern Indian subcontinent: Stable isotopic evidence from paleosols: Geological Society of America Bulletin, v. 107, no. 12, p. 1381–1397, doi: 10.1130/0016-7606(1995)107<1381.

Quade, J., and Cerling, T., 1995, Expansion of C4 grasses in the Late Miocene of Northern Pakistan: evidence from stable isotopes in paleosols: Palaeogeography, Palaeoclimatology, Palaeoecology, v. 115, p. 91–116.

Quade, J., Cerling, T.E., and Bowman, J., 1989, Development of the Asian monsoon revealed by marked ecological shift during the latest Miocene in northern Pakistan: Nature, v. 342, p. 163–166.

Quade, J., Eiler, J., Daëron, M., and Achyuthan, H., 2013, The clumped isotope geothermometer in soil and paleosol carbonate: Geochimica et Cosmochimica Acta, v. 105, p. 92, doi: 10.1016/j.gca.2012.11.031.

Raich, J., and Schlesinger, W., 1992, The global carbon dioxide flux in soil respiration and its relationship to vegetation and climate: Tellus B, v. 44B, p. 81–99.

Retallack, G.J., 2005, Pedogenic carbonate proxies for amount and seasonality of precipitation in paleosols: Geology, v. 33, no. 4, p. 333–336, doi: 10.1130/G21263.1.

Sanyal, P., Bhattacharya, S.., Kumar, R., Ghosh, S.., and Sangode, S.., 2004, Mio–Pliocene monsoonal record from Himalayan foreland basin (Indian Siwalik) and its relation to vegetational change: Palaeogeography, Palaeoclimatology, Palaeoecology, v. 205, no. 1-2, p. 23–41, doi: 10.1016/j.palaeo.2003.11.013.

Seki, O., Foster, G.L., Schmidt, D.N., Mackensen, A., Kawamura, K., and Pancost, R.D., 2010, Alkenone and boron-based Pliocene pCO2 records: Earth and Planetary Science Letters, v. 292, no. 1-2, p. 201–211, doi: 10.1016/j.epsl.2010.01.037.

Sotnikova, M., Dodonov, A., and Pen'kov, A., 1997, Upper Cenozoic bio-magnetic stratigraphy of Central Asian mammalian localities: Palaeogeography, Palaeoclimatology, Palaeoecology, v. 133, p. 243–258.

Suits, N.S., Denning, A.S., Berry, J.A., Still, C.J., Kaduk, J., Miller, J.B., and Baker, I.T., 2005, Simulation of carbon isotope discrimination of the terrestrial biosphere: Global Biogeochemical Cycles, v. 19, no. 1, p. GB1017, doi: 10.1029/2003GB002141.

Tipple, B.J., Meyers, S.R., and Pagani, M., 2010, Carbon isotope ratio of Cenozoic CO2: A comparative evaluation of available geochemical proxies: Paleoceanography, v. 25, no. 3, doi: 10.1029/2009PA001851.

Tripati, A.K., Roberts, C.D., and Eagle, R.A., 2009, Coupling of CO2 and ice sheet stability over major climate transitions of the last 20 million years: Science, v. 326, no. 5958, p. 1394–1397, doi: 10.1126/science.1178296.

Vangengeim, E.A., Vislobokova, I.A., Godina, A.Y., Dimitrieva, E.L., Zhegallo, V.I., Sotnikova, M. V., and Tleuberdina, P.A., 1993, On the Age of Mammalian Fauna from the Karabulak Formation of the Kalmakpai River (Zaisan Depression, Eastern Kazakhstan): Stratigraphy and Geological Correlation, v. 1, no. 2, p. 165–171.

Vislobokova, I.A.A., 1990, On artiodactyls from the Lower Miocene of Tagai Bay of Olkhon Island (Baikal): Paleontological Journal, v. 24, no. 2, p. 134–138.

Vorob'eva, G.A., Mats, V.D., and Shimaraeva, M.K., 1987, Pliocene-Eopleistocene soil formation in the Baikal area: Soviet Geology and Geophysics, v. 28, no. 9, p. 17–24.

Wang, X., Qiu, Z.-D., Li, Q., Tomida, Y., Kimura, Y., Tseng, Z.J., and Wang, H.-J., 2009, A new early to late Miocene fossiliferous region in central Nei Mongol: Lithostratigraphy and biostratigraphy in Aoerban strata: Vertebrata PalAsiatica, v. 47, p. 111–134.

Wang, X., Qiu, Z., and Opdyke, N.D., 2003, Litho-, Bio-, and Magnetostratigraphy and Paleoenvironment of Tunggur Formation (Middle Miocene) in Central Inner Mongolia, China: American Museum Novitates, v. 3411, no. 3411, p. 1–31, doi: 10.1206/0003-0082(2003)411<0001:LBAMAP>2.0.CO;2.

Zhang, Y.G., Pagani, M., Liu, Z., Bohaty, S.M., and Deconto, R., 2013, A 40-million-year history of atmospheric CO2: Philosophical Transactions of the Royal Society A, v. 371.

Zhang, Z., Zhao, M., Lu, H., and Faiia, A.M., 2003, Lower temperature as the main cause of C4 plant declines during the glacial periods on the Chinese Loess Plateau: Earth and Planetary Science Letters, v. 214, no. 3-4, p. 467–481, doi: 10.1016/S0012-821X(03)00387-X.
Zhuang, G., Hourigan, J.K., Koch, P.L., Ritts, B.D., and Kent-Corson, M.L., 2011, Isotopic constraints on intensified aridity in Central Asia around 12Ma: Earth and Planetary Science Letters, v. 312, no. 1-2, p. 152–163, doi: 10.1016/j.epsl.2011.10.005.

***6) Data Repository Figures**:*

DR Figure 1: Compilation of proxy estimates of atmospheric pCO_2 over the Neogene. Black line is a best-fit kernel-smooth (Epanechnikov kernel) with a 1 Myr bandwidth. Black, dashed lines are 1 standard deviation uncertainty on the kernel-smooth (following Gao et al. (2015)). Error bars on individual measurements are from the original publication or the revised estimates of Beerling and Royer (2011). The 1 standard deviation uncertainty is not propagated into the calculation of ϕ_s in the main text, but the sensitivity to this standard deviation is explored in the sensitivity analysis (DR Section 4 and DR Figure 3).

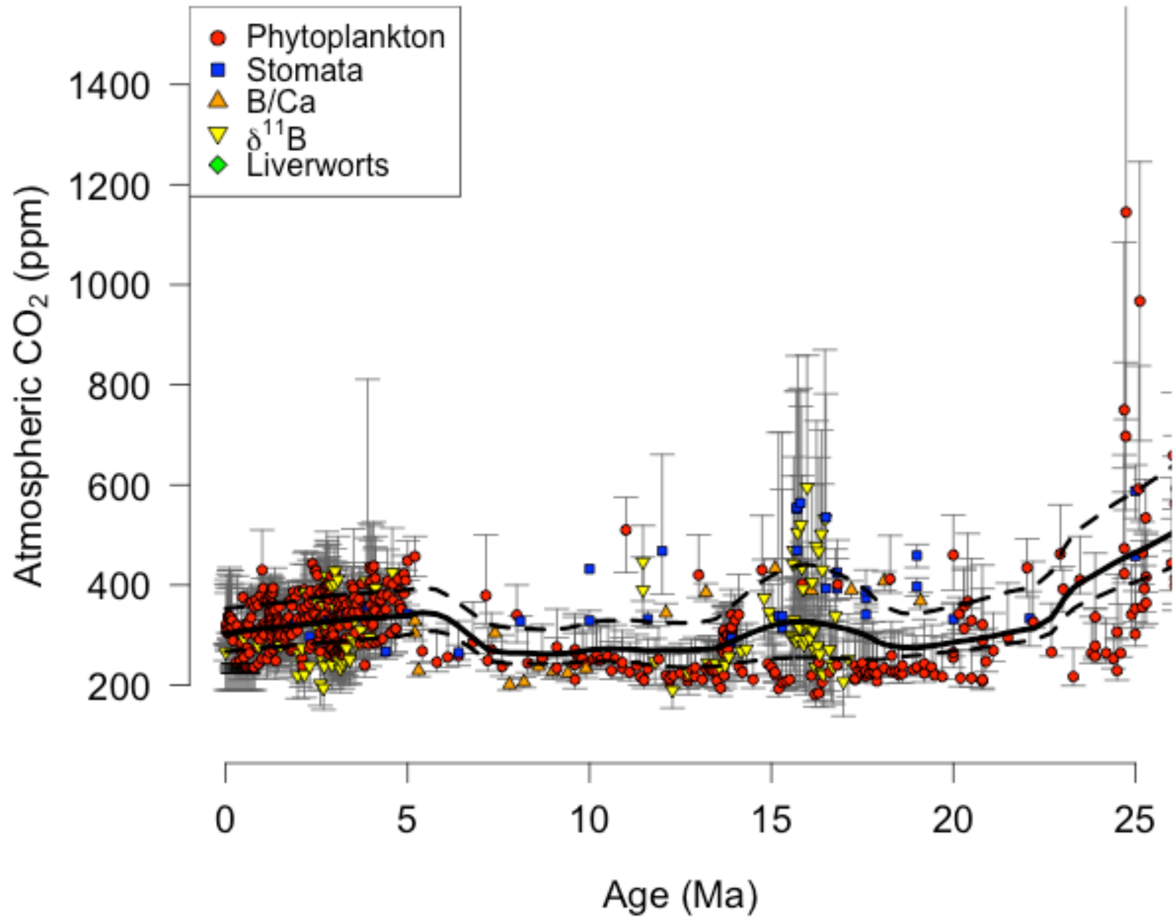

DR Figure 2: Atmospheric CO_2 $\delta^{13}C$ during the Neogene, estimated from the $\delta^{13}C$ of benthic and planktonic foraminifera. Solid line is used in the main text and is the best-guess estimate from Tipple et al. (2010). Dashed lines are upper and lower bounds. Data are re-plotted from Tipple et al. (2010). The upper and lower bounds are not propagated into the calculation of ϕ_s in the main text, but the sensitivity to this standard deviation is explored in the sensitivity analysis (DR Section 4 and DR Figure 4).

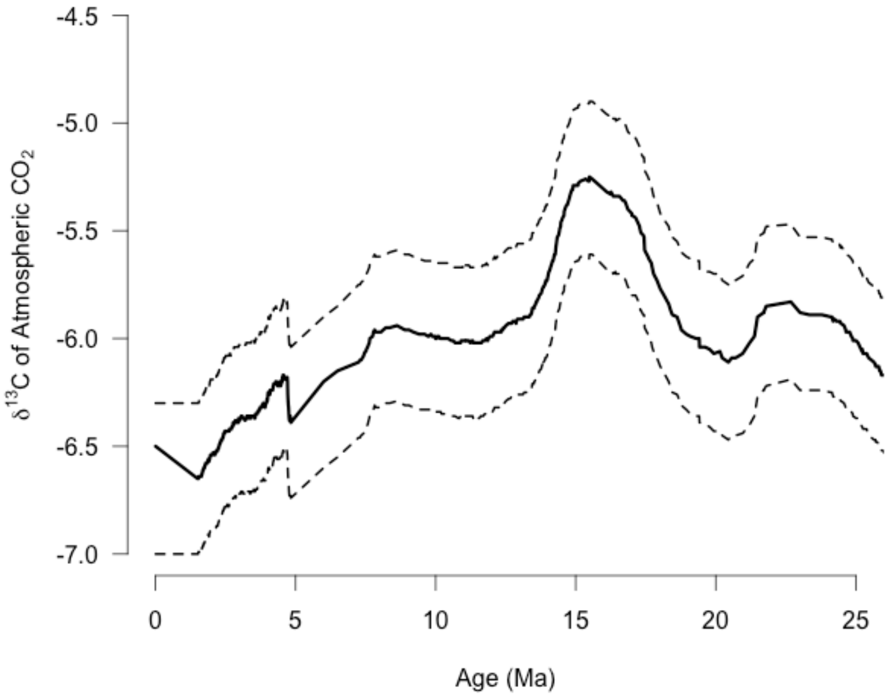

DR Figure 3: Sensitivity of soil respiration to the assumed evolution of pCO_2 (C_a) over the Neogene. "Low Atm CO_2" (A-D) uses the lower, dashed line from DR Figure 1. "High Atm CO_2" (I-L) uses the upper, dashed line from DR Figure 1. "Mean Atm CO_2" (E-H) is the same as presented in the main text and uses the solid, black line from DR Figure 1.

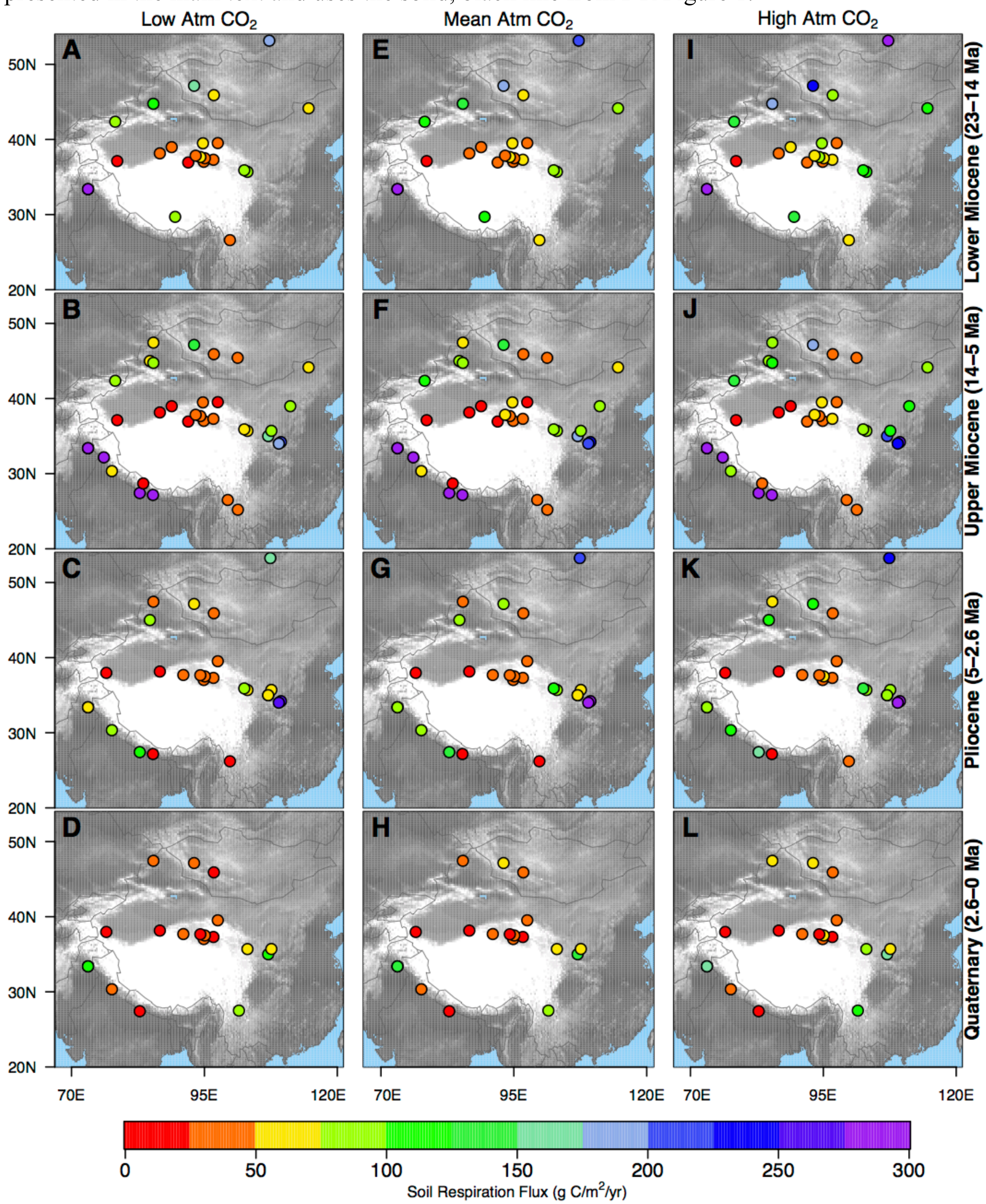

DR Figure 4: Sensitivity of soil respiration to the assumed evolution of δ_a over the Neogene, based on the uncertainty of δ_a from Tipple et al. (2010). "Low Atm CO_2 $\delta^{13}C$" (A-D) uses the lower, dashed line from DR Figure 2. "High Atm CO_2 $\delta^{13}C$" (I-L) uses the upper, dashed line from DR Figure 2. "Mean Atm CO_2 $\delta^{13}C$" (E-H) is also presented in the main text and uses the black, solid line from DR Figure 2.

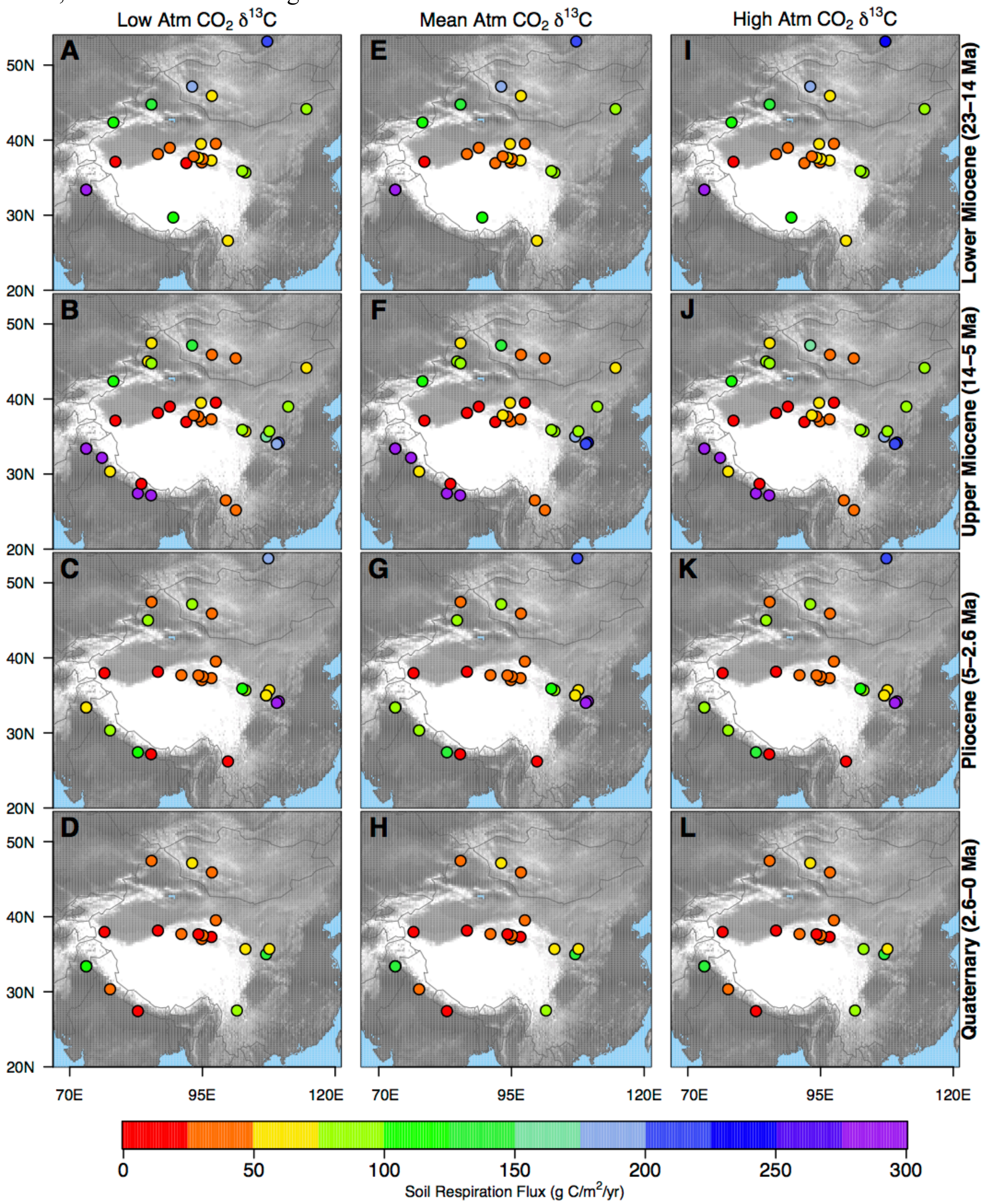

DR Figure 5: Sensitivity of soil respiration to δ_o. Panels A-D use a δ_o of -27‰; panels I-L use a δ_o of -23‰; and, panels E-H are presented in the main text and use a δ_o of -25‰.

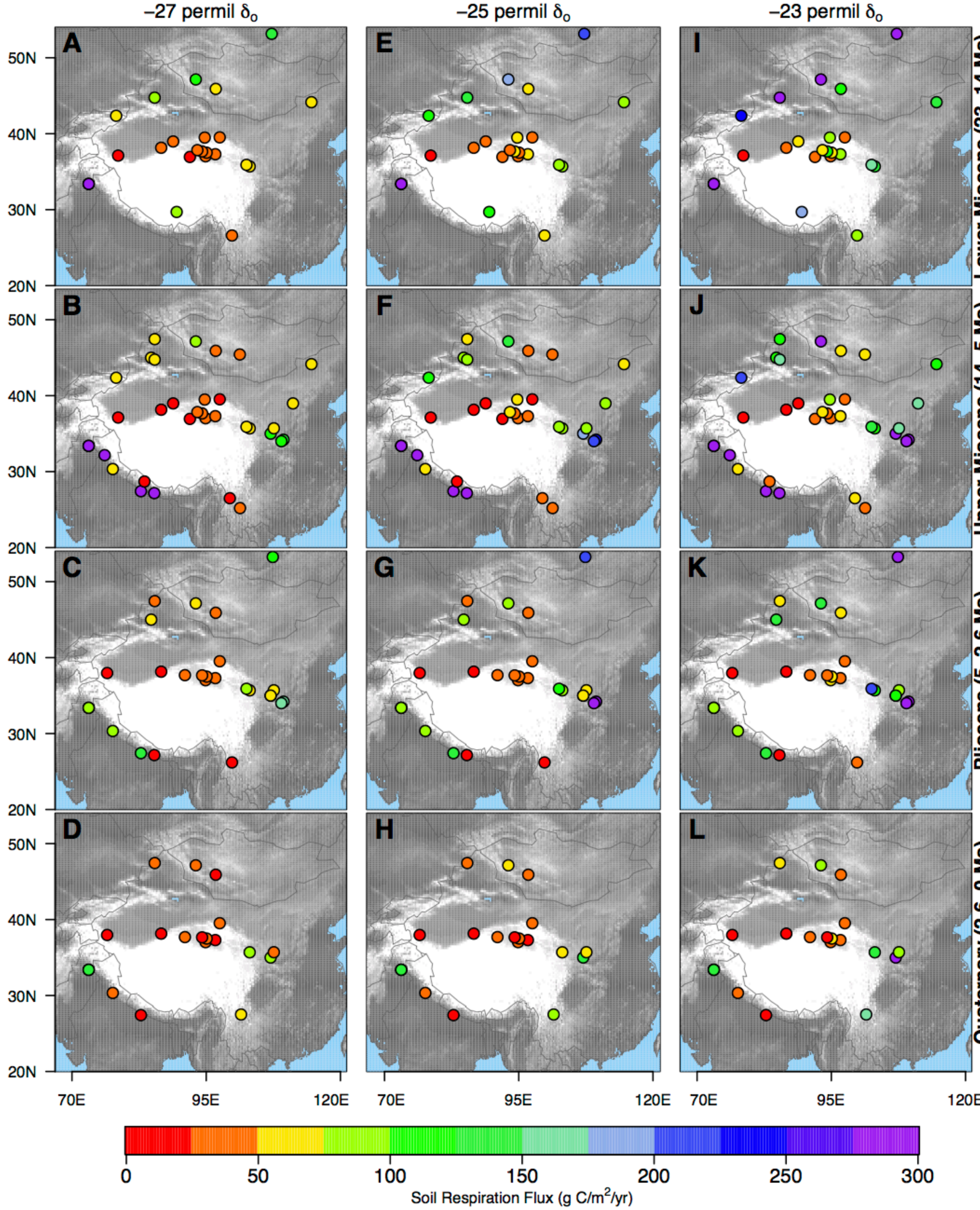

DR Figure 6: Sensitivity of soil respiration to depth of carbonate formation (z). Panels E-H are also presented in the main text.

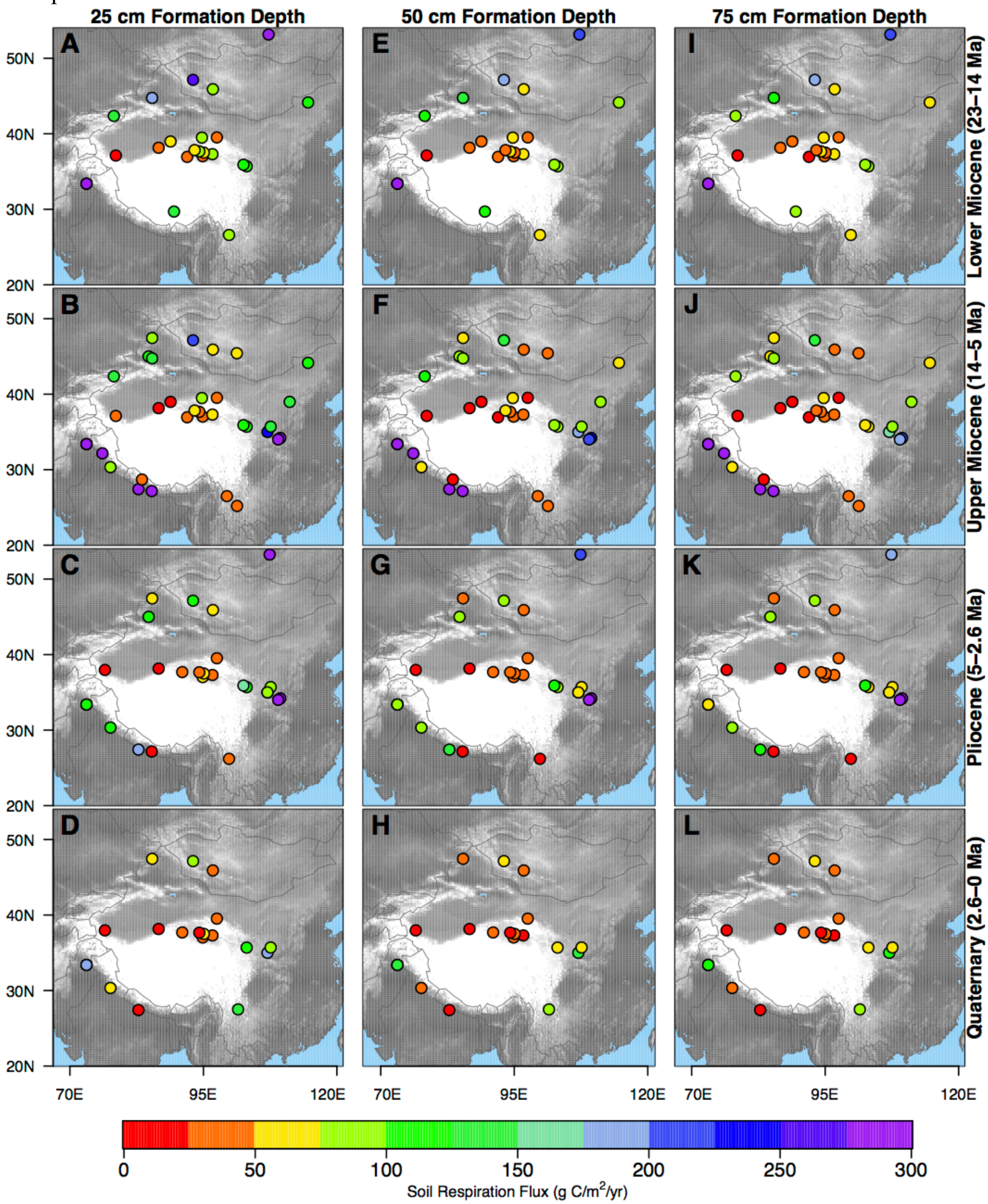

DR Figure 7: Sensitivity of soil respiration to changes in $\dot{z}$ (*i.e.*, z-dot). Panels E-H are also presented in the main text.

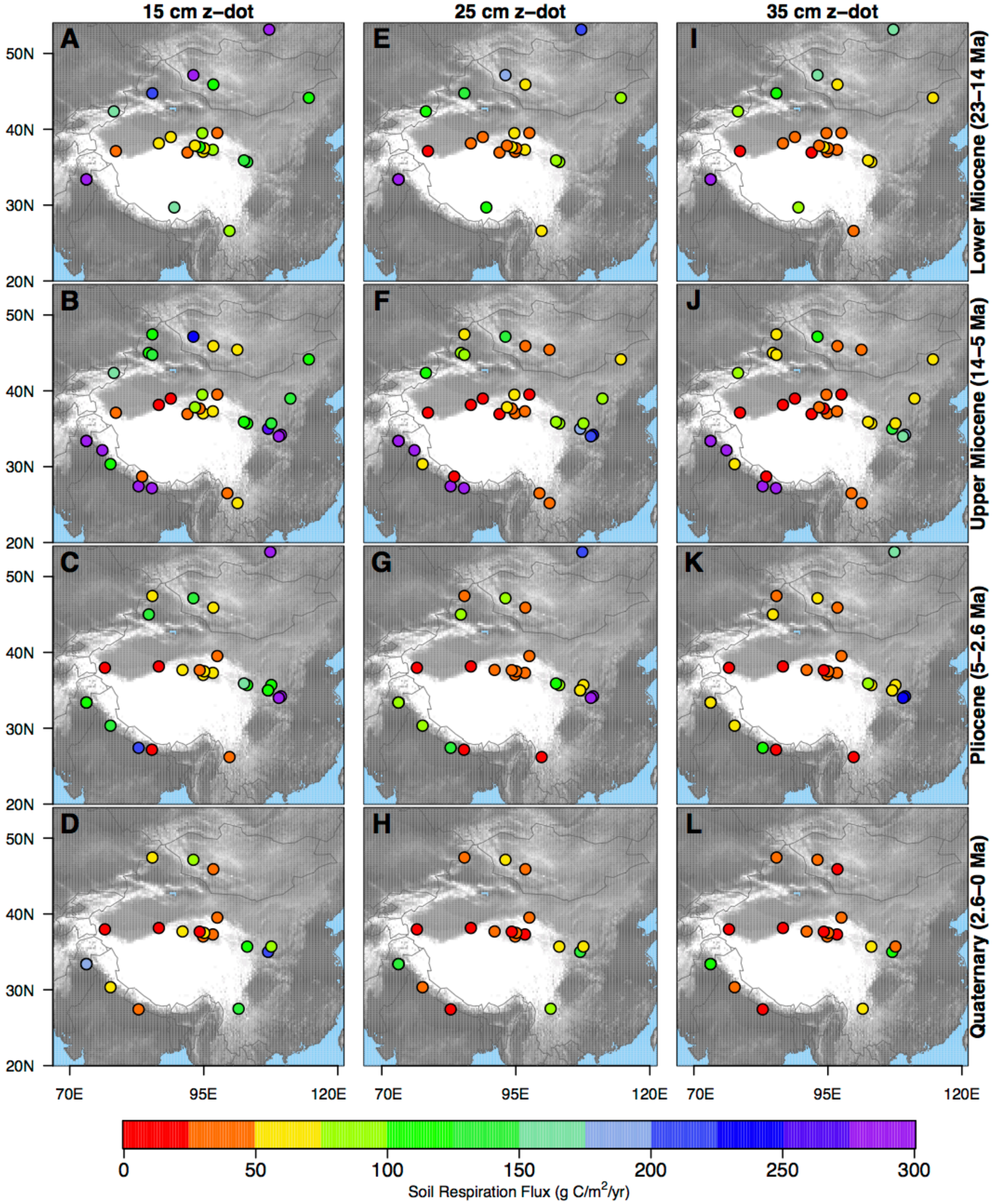

DR Figure 8: Sensitivity of soil respiration to depth of the soil column (*L*). Panels E-H are also presented in the main text.

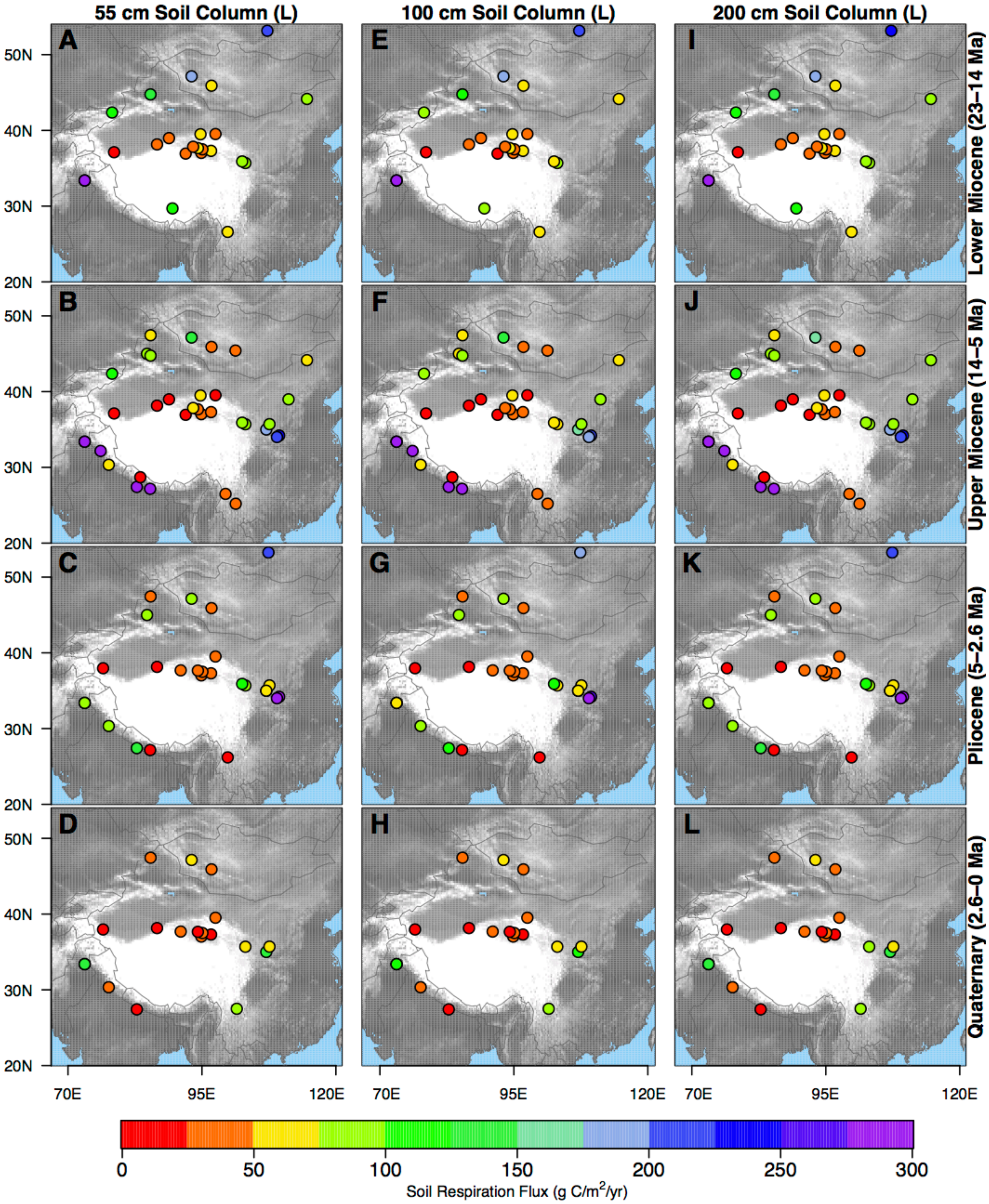

DR Figure 9: Sensitivity of soil respiration to the temperature of carbonate formation (*T*). Panels A-D use the annual average 2 m surface air temperature for each locality, derived from NCEP/NCAR Reanalysis II data (Kanamitsu et al., 2002). Panels I-L use the JJA (June, July, and August) average 2 m surface air temperature for each locality, also derived from NCEP/NCAR Reanalysis II data. Panels E-H are also presented in the main text and use 25°C for all localities.

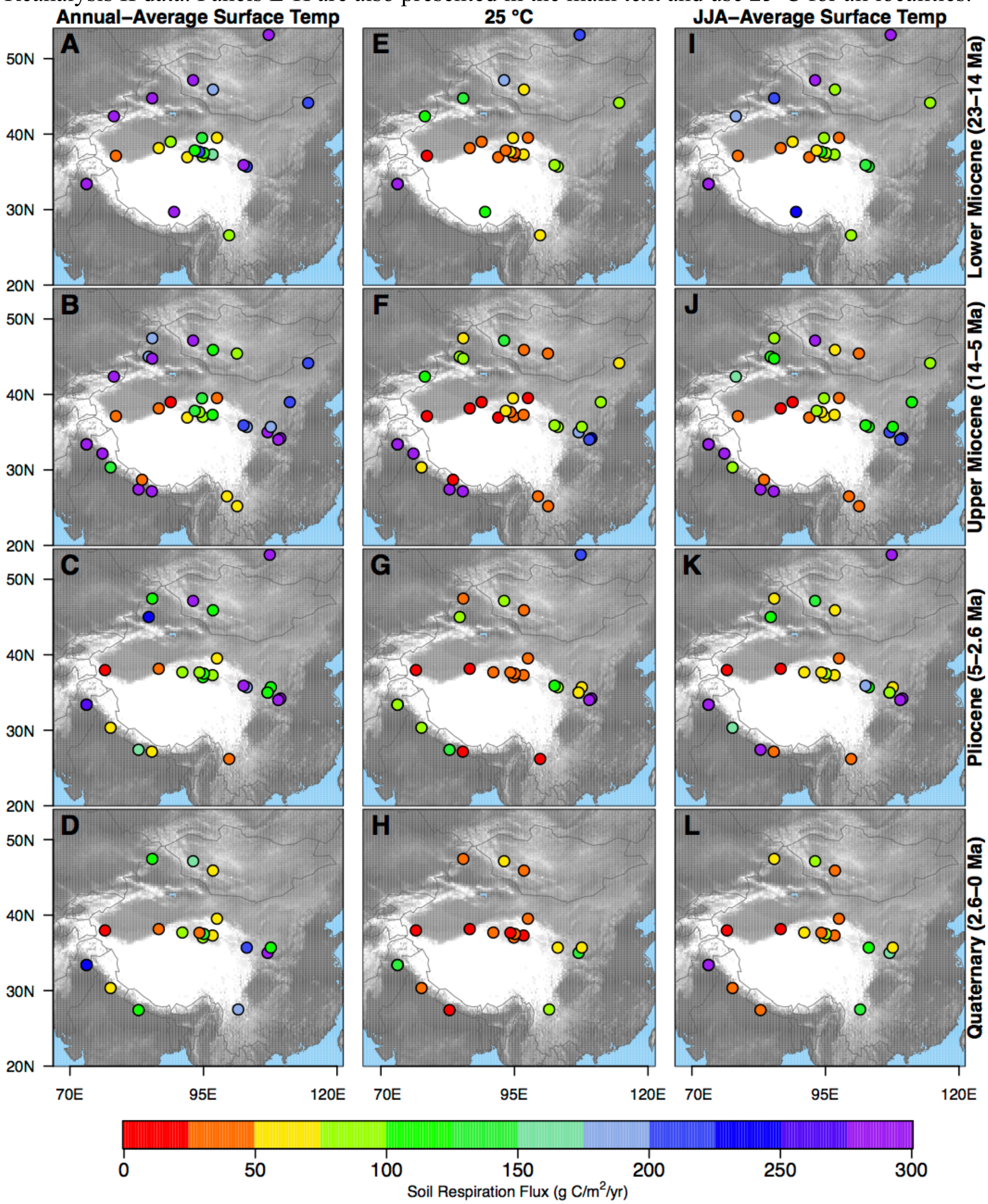

7) DR Tables

DR Table 1: Parameters used in equations 1 and 2 (main text) and equation DR 1 to calculate soil respiration (ϕ_s).

Parameter	Value	Units	Description	Source
D_s	0.042	cm^2/s	Diffusional constant for CO_2 in soil	Cerling and Quade (1993)
ε	0.6	–	Porosity	Cerling and Quade (1993)
L	100	cm	Depth of soil	
z	50	cm	Depth of carbonate formation	Retallack (2005); Cerling and Quade (1993)
$\dot{z}$	25	cm	Characteristic decay depth of soil respiration	Cerling and Quade (1993)
δ_o	-25	‰	$\delta^{13}C$ of soil-respired organic matter[1]	Montañez (2013)
T	25	°C	Temperature of carbonate formation[2]	
δ_a	variable	‰	Atmospheric $\delta^{13}C$	Tipple et al. (2010)
C_a	variable	‰	Atmospheric pCO_2	See full ref list in DR Section 3

[1]For samples from the Siwalik Fm., published measurements of δ_o were used, rather than a spatially-invariant, assumed value of -25‰. See DR Section 3 for more details and a list of references and DR Section 4 and DR Figure 5 for a sensitivity analysis regarding this assumption.

[2]We choose 25°C as the temperature of carbonate formation due to evidence that soil carbonates form during the hottest months of the year (Hough et al., 2014; Quade et al., 2013). We present maps of the sensitivity of soil respiration to this parameter in DR Figure 9.

DR Table 2: Samples collected for this study and organized by location. $\delta^{18}O$ is reported relative to VSMOW; $\delta^{13}C$ is reported relative to VPDB. Estimated age assumes constant sedimentation rates within each formation/member, bound by the minimum and maximum age. The minimum and maximum ages are determined by the bio- and magneto-stratigraphy (detailed in DR Section 1).

Sample #	Height (m)	Age (Ma)	Minimum Age (Ma)	Maximum Age (Ma)	$\delta^{18}O$	$\delta^{13}C$	Material	Formation/Member
				Erlian Basin, Inner Mongolia, China				
				Aoerban (43.3°N; 113.9°E)				
19	29.4	15.9	15.0	20.5	22.7	-5.4	Paleosol	Upper Red
17B	27.4	16.3	15.0	20.5	22.3	-5.8	Paleosol	Upper Red
17A	27.4	16.3	15.0	20.5	22.4	-5.8	Paleosol	Upper Red
18	26.4	16.5	15.0	20.5	22.5	-5.5	Paleosol	Upper Red
16	21.4	17.5	15.0	20.5	21.9	-6.1	Paleosol	Upper Red
15	20.4	17.7	15.0	20.5	21.8	-5.4	Paleosol	Upper Red
14	2.5	18.1	15.0	20.5	22.4	-5.8	Paleosol	Upper Red
13	15.9	18.5	15.0	20.5	22.1	-6.9	Paleosol	Middle Green
12	15.2	18.6	15.0	20.5	22.2	-6.8	Paleosol	Middle Green
11	13.7	18.8	15.0	20.5	22.3	-6.5	Paleosol	Middle Green
10B	11.7	19.1	15.0	20.5	21.9	-5.7	Paleosol	Lower Red
10A	11.4	19.2	15.0	20.5	21.9	-5.8	Paleosol	Lower Red
9	8.4	19.5	15.0	20.5	21.4	-5.6	Paleosol	Lower Red
8B	6.9	19.7	15.0	20.5	20.9	-7.1	Paleosol	Lower Red
8A	6.4	19.7	15.0	20.5	21.3	-6.2	Paleosol	Lower Red
7B	6.3	19.8	15.0	20.5	21.3	-6.2	Paleosol	Lower Red
7A	5.8	19.8	15.0	20.5	20.9	-6.3	Paleosol	Lower Red
6B	5.5	19.9	15.0	20.5	20.9	-6.0	Paleosol	Lower Red
6A	5.0	19.9	15.0	20.5	21.3	-6.1	Paleosol	Lower Red
5A	4.5	20.0	15.0	20.5	20.8	-5.6	Paleosol	Lower Red
5B	4.0	20.0	15.0	20.5	21.7	-5.7	Paleosol	Lower Red
4	3.0	20.1	15.0	20.5	21.1	-5.7	Paleosol	Lower Red
3	2.8	20.2	15.0	20.5	20.8	-5.9	Paleosol	Lower Red

2	2.0	20.3	15.0	20.5	20.9	-6.6	Paleosol	Lower Red
1B	0.3	20.5	15.0	20.5	21.6	-6.2	Fluvial	Lower Red
1A	0.3	20.5	15.0	20.5	22.4	-5.9	Fluvial	Lower Red
0A	0.0	20.5	15.0	20.5	21.1	-5.6	Paleosol	Lower Red
0B	0.0	20.5	15.0	20.5	21.7	-6.5	Paleosol	Lower Red
				Aletexire (43.8°N; 113.1°E)				
19	19.0	11.1	11.0	12.2	23.5	-5.5	Paleosol	Upper Tunggur Fm.
16	16.0	11.2	11.0	12.2	26.3	-4.1	Paleosol	Upper Tunggur Fm.
13B	13.5	11.4	11.0	12.2	23.3	-5.7	Paleosol	Upper Tunggur Fm.
13A	13.0	11.4	11.0	12.2	23.4	-3.8	Paleosol	Upper Tunggur Fm.
11A	11.0	11.5	11.0	12.2	23.5	-5.7	Paleosol	Upper Tunggur Fm.
11B	11.0	11.5	11.0	12.2	23.8	-5.6	Paleosol	Upper Tunggur Fm.
6	6.0	11.8	11.0	12.2	22.8	-6.3	Paleosol	Upper Tunggur Fm.
3	3.0	12.0	11.0	12.2	24.1	-6.5	Paleosol	Upper Tunggur Fm.
1A	1.0	12.1	11.0	12.2	23.1	-6.8	Paleosol	Upper Tunggur Fm.
1B	1.0	12.1	11.0	12.2	24.2	-6.5	Paleosol	Upper Tunggur Fm.
10	9.0	14.0	13.2	15.0	24.5	-6.9	Paleosol	Lower Tunggur Fm.
8	8.0	14.1	13.2	15.0	23.1	-7.7	Paleosol	Lower Tunggur Fm.
7	7.0	14.1	13.2	15.0	24.2	-7.3	Paleosol	Lower Tunggur Fm.
6	5.5	14.2	13.2	15.0	22.7	-8.1	Paleosol	Lower Tunggur Fm.
5	4.5	14.3	13.2	15.0	22.4	-5.6	Paleosol	Lower Tunggur Fm.
4	3.8	14.3	13.2	15.0	22.2	-6.5	Paleosol	Lower Tunggur Fm.
3	3.0	14.3	13.2	15.0	22.0	-7.2	Paleosol	Lower Tunggur Fm.
2	2.5	14.4	13.2	15.0	21.9	-6.8	Paleosol	Lower Tunggur Fm.
1	1.5	14.4	13.2	15.0	22.9	-6.2	Paleosol	Lower Tunggur Fm.
0	0.0	14.5	13.2	15.0	23.2	-6.0	Paleosol	Lower Tunggur Fm.
				Baogeda Ula (44.1°N; 114.60°E)				
7	43.0	6.5	6.0	8.5	22.3	-6.7	Fluvial	Baogedawula
3	42.5	6.5	6.0	8.5	25.8	-6.0	Fluvial	Baogedawula

6	42.0	6.5	6.0	8.5	22.1	-6.9	Fluvial	Baogedawula
4	41.5	6.5	6.0	8.5	21.8	-6.1	Paleosol	Baogedawula
5	41.3	6.5	6.0	8.5	22.0	-6.6	Paleosol	Baogedawula
8B	40.3	6.6	6.0	8.5	22.2	-6.8	Paleosol	Baogedawula
8A	40.3	6.6	6.0	8.5	23.7	-5.0	Paleosol	Baogedawula
9	37.3	6.7	6.0	8.5	25.6	-5.8	Paleosol	Baogedawula
10	24.3	7.4	6.0	8.5	26.5	-4.0	Paleosol	Baogedawula
11	22.3	7.4	6.0	8.5	22.4	-6.7	Fluvial	Baogedawula
12	17.0	7.7	6.0	8.5	22.3	-6.4	Fluvial	Baogedawula
14	15.0	7.8	6.0	8.5	29.6	-5.8	Paleosol	Baogedawula
13	14.0	7.8	6.0	8.5	23.3	-6.0	Fluvial	Baogedawula
15	13.0	7.9	6.0	8.5	28.0	-5.5	Paleosol	Baogedawula
16	12.0	7.9	6.0	8.5	29.3	-5.6	Paleosol	Baogedawula
17	11.0	8.0	6.0	8.5	29.2	-5.5	Paleosol	Baogedawula
18	10.0	8.0	6.0	8.5	21.9	-6.4	Fluvial	Baogedawula
19	8.0	8.1	6.0	8.5	23.0	-6.1	Fluvial	Baogedawula
20	7.0	8.2	6.0	8.5	27.9	-5.8	Fluvial	Baogedawula
21	4.0	8.3	6.0	8.5	24.5	-4.1	Fluvial	Baogedawula
22	0.0	8.5	6.0	8.5	25.1	-4.0	Fluvial	Baogedawula
				Moergan 43.7°N; 112.9°E)				
42	42.0	11.9	11.5	13.2	24.0	-7.1	Paleosol	Upper Tunggur Formation
41	41.0	11.9	11.5	13.2	22.3	-7.6	Fluvial	Upper Tunggur Formation
40A	40.5	11.9	11.5	13.2	22.3	-7.4	Paleosol	Upper Tunggur Formation
40B	40.5	11.9	11.5	13.2	22.7	-7.8	Fluvial	Upper Tunggur Formation
36A	36.0	12.1	11.5	13.2	24.2	-7.8	Paleosol	Upper Tunggur Formation
34.5	34.5	12.1	11.5	13.2	25.2	-7.4	Paleosol	Upper Tunggur Formation
32B	32.9	12.2	11.5	13.2	25.8	-6.3	Paleosol	Upper Tunggur Formation
32C	32.8	12.2	11.5	13.2	23.5	-6.1	Paleosol	Upper Tunggur Formation
32A	32.0	12.2	11.5	13.2	25.7	-6.1	Paleosol	Upper Tunggur Formation
31.5	31.5	12.2	11.5	13.2	22.9	-5.7	Paleosol	Upper Tunggur Formation

27	27.0	12.4	11.5	13.2	22.4	-6.4	Fluvial	Upper Tunggur Formation
27B	27.0	12.4	11.5	13.2	24.5	-6.3	Fluvial	Upper Tunggur Formation
26	26.0	12.4	11.5	13.2	27.5	-4.6	Paleosol	Upper Tunggur Formation
24	24.0	12.5	11.5	13.2	21.4	-6.9	Fluvial	Upper Tunggur Formation
23	23.8	12.5	11.5	13.2	24.1	-5.9	Paleosol	Upper Tunggur Formation
				Zaysan Basin, Kazakhstan				
				Gobi Conglomerate (47.6°N; 84.07°E)				
MOD	–	0.5	0	1	19.9	-5.5	Paleosol	Gobi Conglomerate
3A	–	0.5	0	1	15.1	-4.4	Fluvial	Gobi Conglomerate
3B	–	0.5	0	1	17.1	-3.7	Fluvial	Gobi Conglomerate
3C	–	0.5	0	1	17.8	-3.7	Fluvial	Gobi Conglomerate
28	–	0.5	0	1	15.7	-3.6	Fluvial	Gobi Conglomerate
				Kalmakpay River (47.4°N; 84.4°E)				
4	320.6	5.0	4.5	7.5	15.6	-4.2	Paleosol	Karabulak
5	320.6	5.0	4.5	7.5	16.6	-4.4	Paleosol	Karabulak
7	320.6	5.0	4.5	7.5	19.0	-2.3	Paleosol	Karabulak
2	320.3	5.0	4.5	7.5	17.6	-3.9	Paleosol	Karabulak
1	320.0	5.0	4.5	7.5	17.0	-4.3	Paleosol	Karabulak
6	320.0	5.0	4.5	7.5	16.8	-4.7	Paleosol	Karabulak
31	303.0	5.6	5.0	7.5	14.9	-4.9	Fluvial	Karabulak
30	301.5	5.7	5.0	7.5	17.4	-4.5	Fluvial	Karabulak
29	300.5	5.7	5.0	7.5	14.6	-6.0	Fluvial	Karabulak
28	300.0	5.7	5.0	7.5	14.1	-5.4	Fluvial	Karabulak
27	296.0	5.9	5.0	7.5	17.9	-7.1	Paleosol	Karabulak
26	294.0	5.9	5.0	7.5	18.1	-6.0	Paleosol	Karabulak
25	292.0	6.0	5.0	7.5	17.6	-6.3	Paleosol	Karabulak
24	291.5	6.0	5.0	7.5	16.8	-5.8	Paleosol	Karabulak
23	290.5	6.0	5.0	7.5	17.6	-4.9	Paleosol	Karabulak
21	288.8	6.1	5.0	7.5	17.1	-4.6	Paleosol	Karabulak

20	287.8	6.1	5.0	7.5	15.0	-5.4	Fluvial	Karabulak
19	287.3	6.2	5.0	7.5	16.3	-5.3	Paleosol	Karabulak
18	286.8	6.2	5.0	7.5	17.3	-4.2	Paleosol	Karabulak
17	284.8	6.2	5.0	7.5	17.2	-4.2	Paleosol	Karabulak
16	283.8	6.3	5.0	7.5	19.1	-5.3	Paleosol	Karabulak
15	283.5	6.3	5.0	7.5	18.3	-5.0	Paleosol	Karabulak
14	283.0	6.3	5.0	7.5	19.6	-4.4	Paleosol	Karabulak
13	271.1	6.7	5.0	7.5	16.5	-7.5	Paleosol	Karabulak
11	270.8	6.7	5.0	7.5	16.5	-7.1	Fluvial	Karabulak
12	270.8	6.7	5.0	7.5	16.1	-6.8	Fluvial	Karabulak
10	270.3	6.7	5.0	7.5	15.5	-6.0	Fluvial	Karabulak
8	270.0	6.8	5.0	7.5	15.4	-5.7	Fluvial	Karabulak
9	270.0	6.8	5.0	7.5	15.7	-5.4	Fluvial	Karabulak
87	246.5	7.6	7.5	11.0	21.8	-4.5	Paleosol	Kalmakpay
86	243.5	7.7	7.5	11.0	18.5	-6.0	Paleosol	Kalmakpay
85	240.5	7.8	7.5	11.0	19.9	-5.9	Paleosol	Kalmakpay
84	237.5	7.9	7.5	11.0	20.2	-5.9	Paleosol	Kalmakpay
83	234.5	8.0	7.5	11.0	20.6	-5.1	Paleosol	Kalmakpay
82	231.5	8.1	7.5	11.0	19.2	-5.9	Paleosol	Kalmakpay
81	228.5	8.2	7.5	11.0	18.8	-5.4	Paleosol	Kalmakpay
80	225.5	8.3	7.5	11.0	20.4	-5.9	Paleosol	Kalmakpay
79	222.5	8.4	7.5	11.0	16.4	-5.9	Paleosol	Kalmakpay
78	219.5	8.5	7.5	11.0	20.6	-5.6	Paleosol	Kalmakpay
77	216.5	8.6	7.5	11.0	19.5	-5.5	Paleosol	Kalmakpay
76	215.0	8.7	7.5	11.0	20.8	-4.9	Paleosol	Kalmakpay
75	213.5	8.7	7.5	11.0	20.4	-4.3	Paleosol	Kalmakpay
74	212.0	8.8	7.5	11.0	20.8	-5.5	Paleosol	Kalmakpay
73	210.5	8.8	7.5	11.0	20.8	-5.0	Paleosol	Kalmakpay
72	209.0	8.9	7.5	11.0	20.9	-4.8	Paleosol	Kalmakpay
71	207.5	8.9	7.5	11.0	19.9	-5.0	Paleosol	Kalmakpay
70	206.0	9.0	7.5	11.0	20.7	-7.3	Paleosol	Kalmakpay

69	204.5	9.0	7.5	11.0	21.5	-5.3	Paleosol	Kalmakpay
68	203.0	9.1	7.5	11.0	21.1	-7.6	Paleosol	Kalmakpay
67	201.5	9.1	7.5	11.0	21.0	-5.0	Paleosol	Kalmakpay
66	200.0	9.2	7.5	11.0	20.0	-5.2	Paleosol	Kalmakpay
65	198.5	9.2	7.5	11.0	20.4	-6.8	Paleosol	Kalmakpay
64	197.0	9.3	7.5	11.0	19.2	-6.6	Paleosol	Kalmakpay
63	195.5	9.3	7.5	11.0	20.8	-6.0	Paleosol	Kalmakpay
62	194.0	9.4	7.5	11.0	21.0	-6.1	Paleosol	Kalmakpay
61	192.5	9.4	7.5	11.0	21.7	-5.6	Paleosol	Kalmakpay
60	191.0	9.5	7.5	11.0	21.2	-5.6	Paleosol	Kalmakpay
59	189.5	9.5	7.5	11.0	21.2	-5.4	Paleosol	Kalmakpay
58	188.0	9.6	7.5	11.0	20.5	-5.3	Paleosol	Kalmakpay
57	186.5	9.7	7.5	11.0	20.9	-5.7	Paleosol	Kalmakpay
56	185.0	9.7	7.5	11.0	20.9	-5.9	Paleosol	Kalmakpay
55	183.5	9.8	7.5	11.0	22.4	-5.3	Paleosol	Kalmakpay
54	182.0	9.8	7.5	11.0	21.7	-5.7	Paleosol	Kalmakpay
53	181.5	9.8	7.5	11.0	21.6	-6.2	Paleosol	Kalmakpay
52	180.0	9.9	7.5	11.0	22.2	-6.5	Paleosol	Kalmakpay
51	170.0	10.2	7.5	11.0	19.1	-7.4	Fluvial	Kalmakpay
50	161.5	10.5	7.5	11.0	20.9	-6.3	Paleosol	Kalmakpay
48	157.5	10.7	7.5	11.0	22.1	-5.3	Paleosol	Kalmakpay
46	153.5	10.8	7.5	11.0	19.1	-6.1	Paleosol	Kalmakpay
47	153.5	10.8	7.5	11.0	21.8	-6.7	Paleosol	Kalmakpay
45	148.5	11.0	7.5	11.0	21.7	-6.0	Paleosol	Kalmakpay
44	148.0	11.0	7.5	11.0	21.9	-5.5	Paleosol	Kalmakpay
43	145.0	11.1	7.5	11.0	21.4	-6.0	Paleosol	Kalmakpay
41	142.0	11.2	7.5	11.0	19.7	-5.8	Paleosol	Kalmakpay
40	139.0	11.3	7.5	11.0	20.6	-6.0	Paleosol	Kalmakpay
38	136.0	11.4	7.5	11.0	20.7	-5.9	Paleosol	Kalmakpay
37	133.0	11.5	7.5	11.0	20.1	-8.0	Paleosol	Kalmakpay

				Olkhon Island, Lake Baikal, Russia				
				Kharbay Locality (53.25°N; 107.4°E)				
KHAR2	–	4.5	4.0	5.0	19.0	-8.3	Paleosol	Sasa
KHAR1	–	4.5	4.0	5.0	20.0	-9.0	Paleosol	Sasa
				Tagay Locality (53.15°N; 107.2°E)				
TAG3	–	17.0	11.0	23.0	20.8	-8.5	Paleosol	Tagay
TAG2	–	17.0	11.0	23.0	21.1	-9.0	Paleosol	Tagay
TAG1	–	17.0	11.0	23.0	21.4	-9.3	Paleosol	Tagay

DR Table 3: Calculated mean $\delta^{13}C_c$ (‰ relative to VPDB) and soil respiration (g C/m^2/yr) used to make Figure 2. "5-95%" refers to the range of the 90% confidence interval on the soil respiration estimate. *n* refers to the number of samples included in the calculation. Ages (Ma) column refers to the age range of the data. A single age in this column indicates that no stratigraphic position was given and only an approximate age was reported.

Lower Miocene (23–14 Ma)

Locality	**Latitude**	**Longitude**	**$\delta^{13}C_c$**		**Soil Respiration**		**n**	**Ages**	**Publication**
	°N	**°E**	**mean**	**1σ**	**g C/m^2/yr**	**5-95%**		**Ma**	
Biger Noor	45.9	96.78	-5.2	0.9	74	52-98	11	14.7-23	Caves et al. (2014)
Dzereg	47.14	93.06	-8.5	1.0	211	109-332	15	14.1-20	Caves et al. (2014)
Erlian Basin	44.15	114.6	-6.2	0.7	89	70-127	37	14.1-20.5	This study
Hexi Corridor	39.52	97.52	-2.6	1.2	35	24-44	6	14.4-19.1	Kent-Corson et al. (2009)
Huaitoutala	37.3	96.7	-4.3	1.1	62	40-97	19	14-15.7	Zhuang et al. (2011)
Issyk Kul	42.36	78.23	-6.7	1.2	117	67-193	38	14.1-22.9	Macaulay et al. (2016)
Janggalsay	38.15	86.62	-2.9	1.2	39	19-62	49	14.2-22.9	Kent-Corson et al. (2009)
Jianchuan	26.6	99.8	-3.9	2.1	61	23-116	14	15-15	Hoke et al. (2014)
Jingou	44.75	85.4	-7.3	1.6	149	72-269	53	14.1-22.8	Charreau et al. (2012)
Lake Mahai	37.66	94.24	-5.0	1.9	73	45-106	4	14.5-18.6	Kent-Corson et al. (2009)
Lao Mangnai	36.94	91.96	-1.9	0.9	28	18-40	20	14.2-22.9	Kent-Corson et al. (2009)
Lenghu	37.84	93.36	-4.1	0.3	49	49-49	3	17.4-18.8	Kent-Corson et al. (2009)
Linxia Basin	35.69	103.1	-6.2	0.3	91	79-105	5	14-22.5	Dettman et al. (2003)
Lulehe	37.5	95.08	-4.3	0.1	52	50-55	2	21.1-22.1	Kent-Corson et al. (2009)
Miran River	38.98	88.85	-3.3	2.2	49	20-96	23	14.1-22.7	Kent-Corson et al. (2009)
Oiyug Basin	29.7	89.5	-6.8	0.4	119	101-130	7	15.1-15.1	Currie et al. (2005)
Olkhon Island	53.15	107.2	-8.9	0.4	243	206-278	3	17-17	This study
Pakistan Siwaliks	33.39	73.11	-10.0	0.7	642	272-1751	9	14.1-17	Quade and Cerling (1995)
Puska	37.12	78.6	-0.6	0.2	19	15-24	21	14.1-22.7	Kent-Corson et al. (2009)
Xiao Qaidam	37.03	94.88	-2.8	0.9	38	27-55	8	15-22.9	Kent-Corson et al. (2009)
Xishuigou	39.49	94.73	-5.2	0.5	69	54-92	98	14.1-23	Kent-Corson et al. (2009)
Xunhua Basin	35.9	102.5	-6.3	1.1	90	53-166	51	18.3-20.9	Hough et al. (2011)

DR Table 3 (continued)
Upper Miocene (14–5 Ma)

Locality	Latitude	Longitude	$\delta^{13}C_c$		Soil Respiration		n	Ages	Publication
	°N	°E	mean	1σ	g C/m^2/yr	5-95%		Ma	
Bakiya Khola	27.17	85.33	-10.2	3.0	4947	126-4969	44	6.1-10.9	Harrison et al. (1993)
Baode	38.98	111.16	-6.4	1.0	101	63-166	147	5.3-7.3	Passey et al. (2009)
Biger Noor	45.9	96.78	-3.8	0.8	44	34-60	8	5.7-14	Caves et al. (2014)
Duanjiapo	34	109	-8.6	0.4	216	184-257	4	5	He et al. (2012)
Dzereg	47.14	93.06	-7.6	1.6	161	62-363	15	5.2-13.7	Caves et al. (2014)
Erlian Basin	44.15	114.6	-6.0	1.0	80	43-117	47	6.5-14	This study
Haripur	30.34	77.6	-3.6	1.0	74	41-137	6	5.3-6	Sanyal et al. (2004)
Hexi Corridor	39.52	97.52	-1.8	1.1	24	12-33	9	5.9-13.4	Kent-Corson et al. (2009)
Huaitoutala	37.3	96.7	-3.9	1.4	45	21-82	32	9.7-13.9	Zhuang et al. (2011)
Issyk Kul	42.36	78.23	-7.4	0.6	116	94-155	8	11.8-13.7	Macaulay et al. (2016)
Janggalsay	38.15	86.62	-0.7	0.9	16	9-25	50	5.2-14	Kent-Corson et al. (2009)
Jingou	44.75	85.4	-7.0	0.7	103	69-136	80	8.3-14	Charreau et al. (2012)
Kuitan	45	84.75	-6.2	0.8	82	52-115	56	5.2-9.7	Charreau et al. (2012)
Lake Mahai	37.66	94.24	-3.0	0.8	34	24-45	12	5.7-13.1	Kent-Corson et al. (2009)
Lanping	26.5	99.4	-2.6	2.0	35	12-75	16	8	Hoke et al. (2014)
Lantian	34.2	109.4	-9.0	0.5	249	169-448	42	10-15	Kaakinen et al. (2006)
Lao Mangnai	36.94	91.96	-1.9	0.7	25	18-34	15	5.6-13.7	Kent-Corson et al. (2009)
Lenghu	37.84	93.36	-5.0	0.3	56	52-59	3	7.9-12.1	Kent-Corson et al. (2009)
Lingtai	35	107	-8.4	0.5	189	138-276	68	5-7.6	Ding and Yang (2000)
Linxia Basin	35.69	103.1	-5.8	0.6	82	65-107	11	5.7-13.9	Dettman et al. (2003)
Luhe	25.2	101.3	-3.1	2.0	37	12-62	11	8	Hoke et al. (2014)
Miran River	38.98	88.85	1.2	0.9	7	3-17	55	5.2-13.9	Kent-Corson et al. (2009)
Nepal Siwaliks	27.42	82.84	-9.8	2.1	457	104-1054	24	6.6-11.6	Quade et al. (1995)
Pakistan Siwaliks	33.39	73.11	-7.6	4.1	2144	45-7935	55	5-13.6	Quade and Cerling (1995)
Puska	37.12	78.6	-1.3	0.9	20	16-29	20	5.4-13.6	Kent-Corson et al. (2009)
Ranital	32.17	76.09	-10.4	0.9	1042	151-2420	47	6-11	Sanyal et al. (2004)
Taatsin Gol	45.42	101.26	-3.8	0.1	42	41-42	2	13-13	Caves et al. (2014)

Thakkhola	28.7	83.5	-1.3	2.4	24	3-49	17	8	Garzione et al. (2000)
Xiao Qaidam	37.03	94.88	-3.4	0.5	38	32-50	16	5.5-14	Kent-Corson et al. (2009)
Xifeng	35.7	107.6	-6.4	0.2	103	97-111	9	5-5.3	Jiang et al. (2002)
Xishuigou	39.49	94.73	-5.2	0.7	61	42-75	62	9-14	Kent-Corson et al. (2009)
Xunhua Basin	35.9	102.5	-6.1	0.7	85	57-119	78	5-8.6	Hough et al. (2011)
Zaysan Basin	47.44	85.41	-5.7	0.9	73	53-114	71	5-11.5	This study

DR Table 3 (continued)

Pliocene (5–2.6 Ma)

Locality	Latitude	Longitude	$\delta^{13}C_c$		Soil Respiration		n	Ages	Publication
	°N	°E	mean	1σ	g C/m^2/yr	5-95%		Ma	
Aertashi	37.97	76.55	2.0	1.1	5	0-15	33	2.7-5	Kent-Corson et al. (2009)
Bajiazui	35	107	-5.4	0.3	76	66-82	17	4.6-4.6	He et al. (2012)
Bakiya Khola	27.17	85.33	1.7	0.1	16	13-19	3	3.4-3.4	Harrison et al. (1993)
Biger Noor	45.9	96.78	-3.5	0.6	45	34-52	6	3.5-4.8	Caves et al. (2014)
Duanjiapo	34	109	-9.4	0.7	337	174-441	22	4.9-5	He et al. (2012)
Dzereg	47.14	93.06	-6.1	0.4	93	79-107	6	2.8-5	Caves et al. (2014)
Eryuan	26.2	99.8	-1.6	0.7	24	18-32	7	3	Hoke et al. (2014)
Ganchaigou	37.69	91.04	-2.9	1.0	37	22-57	28	2.7-4.9	Kent-Corson et al. (2009)
Haripur	30.34	77.6	-2.0	1.7	94	13-344	12	3-4.8	Sanyal et al. (2014)
Hexi Corridor	39.52	97.52	-2.6	1.3	35	22-47	4	2.8-4.9	Kent-Corson et al. (2009)
Huaitoutala	37.3	96.7	-3.0	1.1	38	18-51	18	2.6-4.5	Zhuang et al. (2011)
Janggalsay	38.15	86.62	-0.5	0.6	17	12-20	5	2.9-5	Kent-Corson et al. (2009)
Kuitun	45	84.75	-5.9	1.3	93	52-144	10	4.6-4.9	Charreau et al. (2012)
Lake Mahai	37.66	94.24	-2.4	1.5	34	19-45	14	2.8-5	Kent-Corson et al. (2009)
Lantian	34.2	109.4	-9.4	0.6	325	198-532	52	2.7-5	Kaakinen et al. (2006)
Lingtai	35	107	-7.1	1.1	133	75-226	79	2.7-5	Ding and Yang (2000)
Linxia Basin	35.69	103.1	-5.7	1.5	85	62-107	2	3.4-3.5	Dettman et al. (2003)
Lulehe	37.5	95.08	-3.8	0.8	49	35-62	13	2.6-5	Kent-Corson et al. (2009)
Nepal Siwaliks	27.42	82.84	-1.6	3.2	141	11-549	20	2.9-4.9	Quade et al. (1995)
Olkhon Island	53.25	107.4	-8.6	0.5	217	189-244	2	4.5	This study
Pakistan Siwaliks	33.39	73.11	0.6	1.4	227	12-711	17	2.7-5	Quade and Cerling (1995)
Xiao Qaidam	37.03	94.88	-3.5	0.8	45	36-52	3	3.4-5	Kent-Corson et al. (2009)
Xifeng	35.7	107.6	-5.1	0.8	71	46-98	58	2.6-5	Jiang et al. (2002)
Xunhua Basin	35.9	102.5	-6.9	0.9	123	72-161	15	3.7-4.8	Hough et al. (2011)
Zaysan Basin	47.44	85.41	-3.6	1.2	47	33-57	6	4.5-5	This study

DR Table 3 (continued)
Quaternary (2.6–0 Ma)

Locality	Latitude	Longitude	$\delta^{13}C_c$		Soil Respiration		n	Ages	Publication
	°N	°E	mean	1σ	g C/m^2/yr	5-95%		Ma	
Aertashi	37.97	76.55	2.1	0.5	2	0-5	12	1.8-2.6	Kent-Corson et al. (2009)
Biger Noor	45.9	96.78	-2.7	0.2	31	31-32	2	0.8-2	Caves et al. (2014)
Dzereg	47.14	93.06	-4.9	1.5	63	46-80	2	0.9-1.9	Caves et al. (2014)
Ganchaigou	37.69	91.04	-2.8	1.3	35	19-60	26	1.7-2.6	Kent-Corson et al. (2009)
Haripur	30.34	77.6	-1.7	1.7	43	10-91	10	1.8-2.6	Sanyal et al. (2004)
Hexi Corridor	39.52	97.52	-3.1	0.5	35	32-39	3	1-2.2	Kent-Corson et al. (2009)
Huaitoutala	37.3	96.7	-1.2	2.0	23	7-49	6	1.8-2.5	Zhuang et al. (2011)
Janggalsay	38.15	86.62	-0.7	1.0	16	12-20	2	1.8-2.3	Kent-Corson et al. (2009)
Lake Mahai	37.66	94.24	-0.7	1.2	17	12-22	2	2.5-2.6	Kent-Corson et al. (2009)
Lingtai	35	107	-7.6	1.0	144	77-200	24	0-2.3	Ding and Yang (2000)
Linxia Basin	35.69	103.1	-5.6	2.5	80	23-145	32	0.2-2.5	Dettman et al. (2003)
Lulehe	37.5	95.08	-4.2	0.5	51	43-59	5	2-2.5	Kent-Corson et al. (2009)
Nepal Siwaliks	27.42	82.84	-2.1	4.7	19	14-24	4	1.4-1.8	Quade et al. (1995)
Pakistan Siwaliks	33.39	73.11	0.8	1.5	477	2-933	36	0.5-2.6	Quade and Cerling (1995)
Xiao Qaidam	37.03	94.88	-3.0	1.1	35	29-42	2	1.8-2.6	Kent-Corson et al. (2009)
Xifeng	35.7	107.6	-5.0	1.1	68	47-103	6	2.4-2.6	Jiang et al. (2002)
Yanyuan	27.5	101.5	-6.5	1.1	103	73-128	3	2.5-2.5	Hoke et al. (2014)
Zaysan Basin	47.44	85.41	-4.2	0.8	48	40-65	5	0.5	This study